## REVIEW

Check for updates

# Synthesis of emerging 2D layered magnetic materials

Mauro Och,[a] Marie-Blandine Martin,[b] Bruno Dlubak, [b] Pierre Seneor[b] and Cecilia Mattevi [b] *[a]

van der Waals atomically thin magnetic materials have been recently discovered. They have attracted enormous attention as they present unique magnetic properties, holding potential to tailor spin-based device properties and enable next generation data storage and communication devices. To fully understand the magnetism in two-dimensions, the synthesis of 2D materials over large areas with precise thickness control has to be accomplished. Here, we review the recent advancements in the synthesis of these materials spanning from metal halides, transition metal dichalcogenides, metal phosphosulphides, to ternary metal tellurides. We initially discuss the emerging device concepts based on magnetic van der Waals materials including what has been achieved with graphene. We then review the state of the art of the synthesis of these materials and we discuss the potential routes to achieve the synthesis of wafer-scale atomically thin magnetic materials. We discuss the synthetic achievements in relation to the structural characteristics of the materials and we scrutinise the physical properties of the precursors in relation to the synthesis conditions. We highlight the challenges related to the synthesis of 2D magnets and we provide a perspective for possible advancement of available synthesis methods to respond to the need for scalable production and high materials quality.

[a]*Department of Materials, Imperial College London, SW72AZ London, UK.*
*E-mail: c.mattevi@imperial.ac.uk*
[b]*Unité Mixte de Physique, CNRS, Thales, Université Paris-Saclay, 91767 Palaiseau, France*

## Introduction

Magnetism and its application in spin electronics have been key to develop high-density data storage solutions. Phenomena such as GMR (giant magnetoresistance) and TMR (tunnel magnetoresistance) effects have been widely used in high efficiency hard drive read heads and have fueled the big data and cloud

era revolution.[1] With the development of fundamental mechanisms such as STT (spin transfer torque) and SOT (spin orbit torque), spintronics technologies have been moving to non-volatile highly efficient and ultra-low power memory circuits such as MRAMs (magnetic random access memories) and are now progressively being integrated to CMOS-based devices for green technologies.[2–5] Next generation spintronics is expected to provide opportunities to merge logic and memory functions in computing architectures under the unified spin variable, as well as in many disruptive approaches for post-CMOS computing such as stochastic, logic-in-memory architectures, neuromorphic, and quantum circuits.[6–14]

All these envisioned applicative exploitations of spin electronics fuel the development of innovative material platforms, which can bring novel functionalities and performance to devices. In particular, 2D materials have been expected to deliver many opportunities to tailor spin-based device properties and bring to light unseen possibilities. One of the first examples is the robust spin transport in graphene (the prototypical 2D material), which unveils the long sought possibility of a platform for spin transport and potential path for spin logics targeting beyond CMOS solutions.[15,16] More remarkably, the development and integration of 2D materials have also been impressive with respect to the basic building block of spintronics, the magnetic tunnel junction (MTJ) at the core of MRAM technology.[17] Within only few years 2D materials have already been demonstrated to provide many outstanding novel properties for spintronics such as: interface protection and stabilisation, diffusion control, spin filtering, atomic control crafting of spinterfaces (ferromagnet/non-magnet interface), increase of perpendicular magnetic anisotropies, natural atom thick interfaces for spin-to-charge conversion and modulation of spin orbit torques.[18–33] Remarkably, while 2D materials already offer a strong materials platform for spin transport

and manipulation towards spin information processing for beyond CMOS, their main potential remains to be unleashed: an unprecedented full control and tailoring of electronic and magnetic properties through gating.[34,35] While the first explorations of 2D materials integration in MTJs concerned only the prototypical 2D materials graphene and h-BN, studies were soon extended to large families of 2D semiconductors such as transition metal dichalcogenides (TMDs).[36–39]

Most of the initial studies exploring 2D materials properties for spintronics were based on atomically thin layers, which were mechanically exfoliated form bulk crystals.[40] This technique is known to enable the isolation of high quality atomically thin 2D materials in a relatively straightforward manner. However, this approach is not scalable and, additionally, is even detrimental for spintronics applications as the exfoliation is carried out in an oxidative environment. This has been a recurring limitation for the integration and study of 2D materials on typical ferromagnetic spin sourcing materials, such as Ni, Co, Fe, and their alloys. Indeed, the surface oxidation of these material quenches the spintronics properties, in turn leading to very limited spin extraction and transport performances in complete spin valve structures. In parallel to the exfoliation approach, the direct growth of 2D materials appears as a crucial to overcome both the issue of scalability and the integration with delicate spintronics materials.[17,19] This has been observed for graphene and h-BN with direct chemical vapour deposition (CVD) growth being central in the unlocking of their spintronics properties.[21,28]

Among 2D materials, 2D ferromagnets (FM) are promising for spintronics as they could lead to a complete 2D MTJ.[41–44] Departure from usual spin sources would allow the exploitation of the 2D material characteristics (conformality, flexibility, atomic thickness control, *etc.*) for spin based circuits. In addition, 2D ferromagnets have been predicted to be half

*Dr Bruno Dlubak graduated from the University of Cambridge and received his PhD from the University of Paris-Sud in 2011 working on graphene spintronics. After a postdoctoral appointment at the University of Cambridge working in John Robertson group, Dr Dlubak joined the Unité Mixte de Physique CNRS-Thales lab, associated to the Paris-Saclay University, becoming a CNRS Researcher in 2014. His current research interests concern the exploration of novel 2D materials for electronics and spintronics devices, with a focus on spin dependent transport and injection in nanostructures and 2D materials.*

**Bruno Dlubak**

*Dr Pierre Seneor received his PhD from Ecole Polytechnique in 2000 under the supervision of A. Fert working on spin dependent tunneling in oxides. After a postdoctoral appointment at the California Institute of Technology, Dr Seneor came back to the Unité Mixte de Physique CNRS/Thales industrial/academic laboratory while joining in 2003 the physics department of University of Paris-Sud (now Paris-Saclay) in Orsay where he is now full professor. He was awarded Junior Fellow of the Institut Universitaire de France excellency institute. His current research interests include exploring the physics of novel molecular and 2D materials in low dimension towards nanoelectronics and spintronics devices.*

**Pierre Seneor**

metallic (meaning only one spin direction is present at the Fermi level) materials,[45,46] *i.e.* the perfect fully polarised spin source. This would naturally offer infinite TMR for a 2D MTJ and has been a long-haul quest in spintronics.[47] Furthermore, magnetism at the 2D limit has barely been exploited in functional structures and promises to provide unseen properties for the control of spin functions. Indeed while ultimately achievable with conventional magnets, reducing thicknesses down to few atoms thick requires sophisticated engineering developments.[48] On the contrary this comes naturally to 2D materials with atomic precision and a wealth of gating opportunities of their magnetic/electronic properties. While the sole existence of spontaneous magnetisation in 2D materials has been questioned by the Mermin–Wagner–Hohenberg (MWH) theorem since the 60s,[49] it is only very recently that intrinsic magnetic order was experimentally observed in ultrathin layers of 2D ferromagnets, such as $CrI_3$, $CrGeTe_3$, and $Fe_3GeTe_2$.[50–55] Compared to conventional ferromagnetic materials used in spintronics, those materials are extreme sensitive to external doping and electromagnetic fields. This gives for the first time the opportunity to play with their intrinsic magnetic and electronic properties, an asset unavailable before. In particular, the gating of 2D magnetic material could pave the way toward magnetic phase crafting at the atomic level and on-the-fly electrical control.

Concerning spintronics devices, the field is just blooming. Fully 2D MTJs based on 2D ferromagnets have been successfully demonstrated using metallic $Fe_3GeTe_2$ and h-BN barriers in $Fe_3GeTe_2$/h-BN/$Fe_3GeTe_2$ heterostructures.[56] Remarkably, a clear TMR of 160% was observed at 4 K leading to a spin polarisation of 66% for the $Fe_3GeTe_2$/h-BN interface (Fig. 1(d–f)). Similarly, $Fe_3GeTe_2$ structures (using $MoS_2$ barriers or spacer-free homojunctions) presented more recently further confirm the interest in those 2D ferromagnets for spintronics.[44,57]

Here, beyond the remarkable observation of high spin polarisation for the $Fe_3GeTe_2$ electrode, one of the outstanding advantages remains to be unleashed and this is the tunability. The Curie temperature ($T_c$) of $Fe_3GeTe_2$ has been shown to be gate tunable and it could potentially reach room temperature.[58] Such a material property holds very strong promise for future applications. For example, one could think of lowering $T_c$ (or change the anisotropy), through gate control, to achieve ultra-low power magnetisation switching and subsequently raise the temperature to obtain long term storage. In addition, most of these new 2D materials naturally offer perpendicular anisotropy, a property usually available only in ultrathin 3D ferromagnets which are inherently more difficult to grow.[59] The advantage of perpendicular magnetic anisotropy is that it withstands downscaling while maintaining thermal stability, which is a requirement for future ultrahigh density devices.[2] Along this way, their intrinsic 2D nature makes them also perfect candidates for hosting controllable topological protected skyrmions,[60] the ultimate spintronics memory element.[61]

Also, in a very promising way, semiconducting $CrI_3$, the flagship of the chromium trihalides family, was reported as an efficient insulating spin-filtering barrier for 2D MTJs. Indeed, its strong spin filtering properties were evidenced for $CrI_3$ sandwiched by two graphene electrodes in a Gr/$CrI_3$/Gr tunnel structure (Fig. 1(a–c)).[41,42,62] The MR in the device relied on the applied magnetic field switching the internal $CrI_3$ interlayer magnetic configuration from antiferromagnetic (AFM) to ferromagnetic in a way mimicking the early GMR behavior. In the AFM state, every second layer of the $CrI_3$ would filter out an opposite spin direction resulting in a large resistance for the tunnel barrier, while with an applied magnetic field all the layers would align. The latter would allow a preferential spin direction to pass through, and thus it would reduce the overall resistance. Very large TMR in the million percent range were found, thanks to the spin filtering high efficiency. Additionally voltage control was also demonstrated highlighting the potential of this type of 2D AFM/FM for future spintronics devices.[63,64] As such a new type of device could arise using 2D FMs to work as a gate-tunable tunneling barrier spin filter. It would rely on the property of tuning the interlayer coupling from ferromagnetic to antiferromagnetic through an external gate voltage, which would be unavailable using conventional FM.[65]

2D insulator/semiconductor ferromagnets could find their way in spin dynamics and more specifically, in the field of magnonics,[66] targeting downscaled optics within magnetic materials through spin waves. In this emerging field, 2D insulator/semiconductor ferromagnets could lead to the demonstration of gate tunable magnonic channels.[67] For example, long distance magnon transport was already demonstrated in 2D antiferromagnetic $MnPS_3$ connected by two Pt spin hall effect injector/detector (Fig. 1(g–i)).[68] Their manipulation by STT and SOT has also been demonstrated in part. Indeed switching of the semiconducting van der Waals ferro-magnet $CrGeTe_3$ through SOT was demonstrated at the interface with Ta.[69] Finally 2D insulator/semiconductor ferromagnets could also tackle the long quest for integrating magnetism into semi-

*Dr Cecilia Mattevi received her Laurea degree in Materials Science from the University of Padua and a PhD in Materials Science from the University of Padua in 2008. After a postdoctoral appointment at Rutgers University, Dr Mattevi joined the Materials Department at Imperial College London, becoming a Junior Research Fellow in 2010 and then a Lecturer and Royal Society University Research Fellow in 2012. Cecilia is a Fellow of the Royal Society of Chemistry and her research interest includes the precise synthesis of 2D materials with tailored characteristics and the investigation of their properties for energy conversion, energy storage, and nanoelectronics.*

**Cecilia Mattevi**
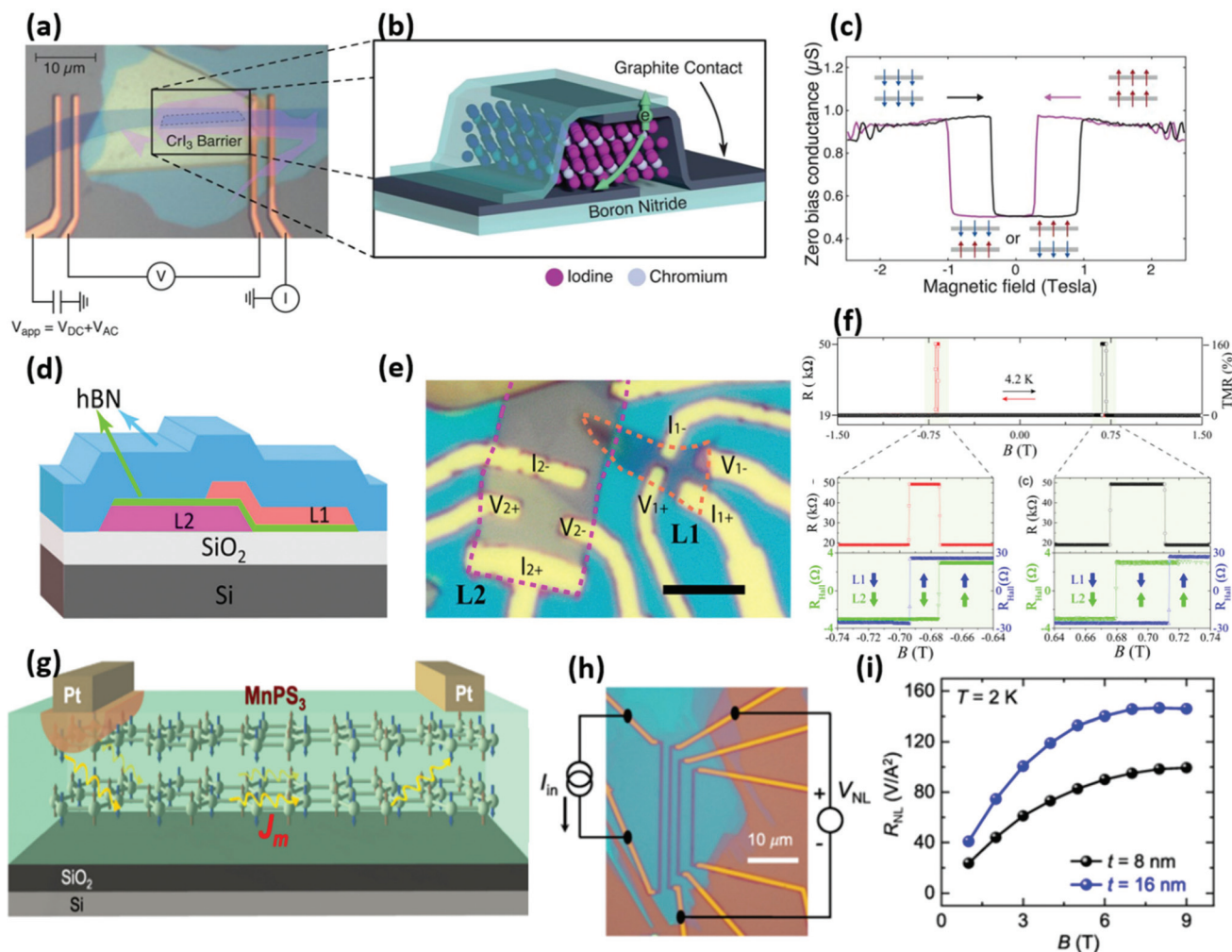
**Fig. 1** 2D magnet-based devices. (a–c) Optical image and schematic of a Gr/CrI₃/Gr MTJ and measured magnetoconductance *vs.* applied magnetic field.[42] Reproduced with permission from ref. 42. Copyright 2018 The American Association for the Advancement of Science. (d–f) Optical image and schematic of a tunnelling spin valve device based on a Fe₃GeTe₂(L1)/h-BN/Fe₃GeTe₂(L2) heterostructure. The measured TMR reaches 160% at $B$ = ± 0.7 T.[56] Scale bar is 5 µm. Reproduced with permission from ref. 56. Copyright 2018 American Chemical Society. (g–i) Schematic and optical image of a magnonic transport-based device using a MnPS₃ bilayer as magnon transport medium from the Pt electrodes, acting as magnon source and detector. The graph shows the nonlocal magnon signal ($R_{NL}$) against the applied magnetic field B for devices of thicknesses 8 and 16 nm at 2 K.[68] Reproduced with permission from ref. 68. Copyright 2019 American Physical Society.

conductors started by diluted magnetic semiconductors.[70] Providing high mobility could be found new 2D ferromagnet semiconductors (such as early highlighted CrSiTe₃ and CrGeTe₃ [54,71]), it might reboot the field in an unexpected way.

While pioneer works in this direction have been based on exfoliated material,[41–44] already unveiling a strong potential for spin performances and functionalities, large scale growth will not only allow the systematic study of their properties but also will enable the direct integration of these materials in heterostructures for the fabrication of functional devices. The integration of 2D magnets grown by CVD in functional spintronics heterostructures can be foreseen to serve to the emerging field of spintronics circuits.

In this article, we review the state of the art of the synthesis of the most investigated 2D materials with magnetic order.

Specifically, we discuss Fe₃GeTe₂ and other ternary tellurides,[72,73] CrX₃ (X = Cl, I, Br) and α-RuCl₃,[74–76] MPX₃ (M = metal, X = S, Se),[77,78] Cr and V dichalcogenides,[79–82] and metal doped TMDs.[83–85] The crystal structure, the electronic and the magnetic properties of these 2D magnets are reported in Table 1. In the first part of this review, we discuss the state of the art of synthesis of 2D magnets followed by a critical discussion of perspective synthetic solution to achieve a control over the materials characteristics. In the last section we discuss the application of metalorganic CVD (MOCVD) for the growth of 2D magnetic materials. Since MOCVD has been recently used for full-scale TMDs synthesis with thickness control,[86,87] we prospect that this technique may lead to similar results for 2D magnets. Moreover, ternary and quaternary alloys and compounds have already been achieved using MOCVD in thin

**Table 1** Crystal models, electronic and magnetic properties of the 2D magnets object of this review

| Crystal | Side view | Top view | Space group | Electronic type | Magnetic type | Magnetic transition temperature (K) |
|---|---|---|---|---|---|---|
| $CrS_2$ | | | $P\bar{3}m1$ | Metallic | AFM | — |
| $CrSe_2$ | | | | | AFM | — |
| $CrTe_2$ | | | | | FM | 219 [88] |
| $VS_2$ | | | | | FM | >330 (f-L) [89] |
| $VSe_2$ | | | | | FM | 300 [90] |
| $VTe_2$ | | | | | FM | — |
| $Fe_3GeTe_2$ | | | $P6_3/mmc$ | Metallic | Ising-FM | 130 [91] |
| $CrCl_3$ | | | $C2/m$ | Insulating | XY-FM | 17 (f-L) [92] |
| $CrI_3$ | | | | | Ising-FM | 45 [51] |
| $CrBr_3$ | | | | | Ising-FM | 34 [93] |
| $FePS_3$ | | | $C2/m$ | Insulating | Ising-AFM | 110 [78] |
| $MnPS_3$ | | | | | Heisenberg-AFM | 78 (5 L) [94] |
| $NiPS_3$ | | | | | XY-AFM | <25 (155 bulk) [95] |
| $FePSe_3$ | | | $R\bar{3}$ | Insulating | Ising-AFM | 119 [96] |
| $MnPSe_3$ | | | | | XY-AFM | 74 [96] |
| $CrSiTe_3$ | | | | | Ising-FM | 32 (bulk) [97] |
| $CrGeTe_3$ | | | | | Heisenberg-FM | 30 [50] |
| $MnBi_2Te_4$ | | | $R\bar{3}m$ | Insulating | Heisenberg-AFM | 25 (bulk) [98] |
| $\alpha$-$RuCl_3$ | | | $P312$ | Semiconductive, direct bandgap 1.9 eV (ref. 99) | Kitaev-AFM | 7 (bulk) [100] |

films industry, and we envision possible pathways to synthesise phosphochalcogenides, binary and ternary tellurides and alloys using this method.

# State of the art of magnetically active 2D crystal growth

### Metal halides

One of the most studied classes 2D magnets are metal halides. These are chlorides, bromides, and iodides of transition metals such as Ti, V, Cr, Mn, Fe, Co and Cu. The majority of them have been predicted to be predominantly antiferromagnetic with two ferromagnetic exceptions, which are $CrI_3$, possessing a Curie temperature of 45 K as reported in Fig. 2(a), and $CrBr_3$.[101] However, only a few of them have been obtained experimentally. Within this group, the Cr-based halides have been the most studied for their magnetic properties and control over their magnetic order has been achieved via gating, doping, pressure and stacking order.[51,74,102–105] Atomically thin flakes were obtained via mechanically exfoliation from chemical vapour transport (CVT) grown bulk crystals (Fig. 3(a)).[106] In this process, Cr powders were placed in an ampoule filled with halogen gas, which is inserted into a furnace (set at 600–700 °C) while the other end is kept at room temperature.[92,107] Here the Cr powders are transported by the convective flux onto the colder end outside the furnace and after several days the slow reaction in the gas phase between Cr atoms with the halogen species yielded high quality bulk crystals. The synthesis of Cr halides alloys has been demonstrated by mixing precursors powders.[108] In specific, $CrCl_{3-x}Br_x$ and $CrBr_{3-x}I_x$ were obtained mixing $CrCl_3$ or $CrBr_3$ commercial powders with Br or I beads according to the desired final stoichiometry. By mixing $Cr_2O_3$ and $CrCl_3$ powders in a similar setup it is possible to obtain the vdW magnetic insulator CrOCl.[109]

A different synthetic approach has been reported by Gamelin et al., who has demonstrated the colloidal synthesis of $CrI_3$, $CrBr_3$ and alloys.[110] $Cr(OCMetBu_2)_3$ and trimethylsilyl halide ($C_3H_9SiX$) have been used as precursors and the new phase of $CrI_3$ and $CrBr_3$ has been obtained via chemical reaction and precipitation occurring at 135–180 °C. The resulting crystals are nanoplatelets (Fig. 3(b)) as large as 26 nm and composed by 4–10 stacked layers. Magnetisation measurements demonstrated a similar behaviour to exfoliated crystals.

Recently, a few studies on the synthesis of $FeCl_2$ and $\alpha$-$RuCl_3$ have been reported. Zhou et al. has demonstrated the
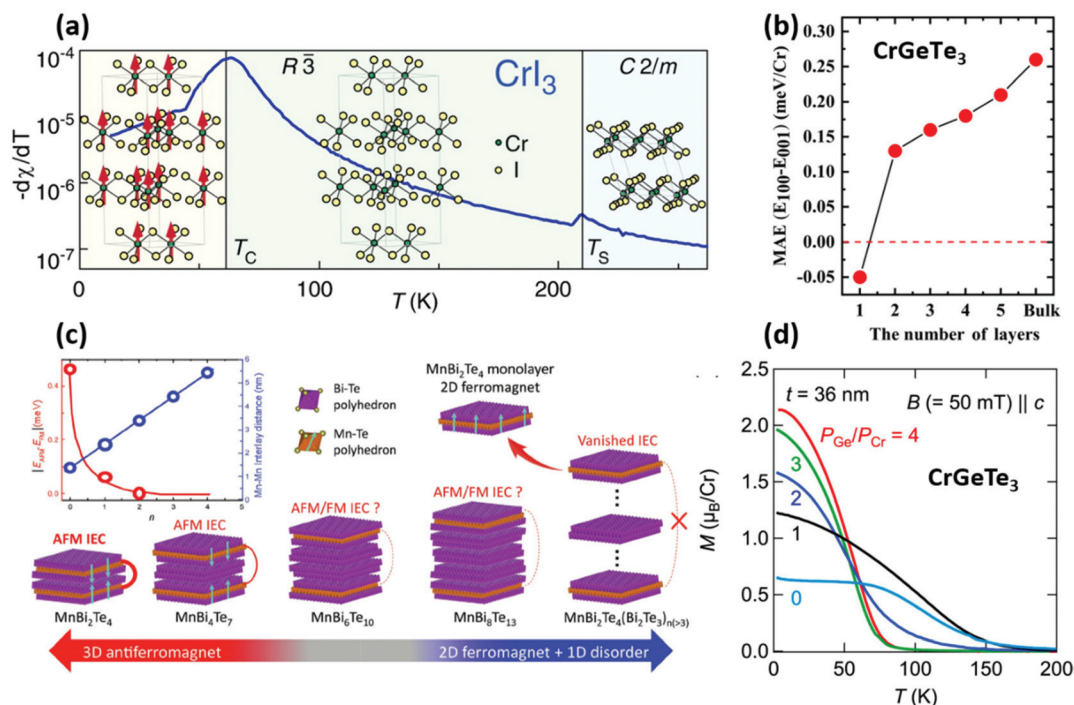
Fig. 2 The role of the structure and the composition of materials in determining the magnetic properties; (a) phase transition of bulk CrI₃. The crystal changes crystallography at 220 K and at 61 K ($T_c$) spins align and magnetisation arises.[107] Reproduced with permission from ref. 107. Copyright 2015 American Chemical Society. (b) Calculated magnetic anisotropy energy (MAE) vs. layer number in CrGeTe₃.[111] Reproduced with permission from ref. 111. Copyright 2019 AIP Publishing. (c) Evolution of the magnetic behaviour in MnBi₂Te₄(Bi₂Te₃)ₙ. The Bi₂Te₃ layers separate the ferromagnetic MnBi₂Te₄ sheets decreasing the magnetic interaction (upper left inset) and decoupling the antiferromagnetism present in bulk.[112] Reproduced with permission from ref. 112. Copyright 2020 John Wiley and Sons. (d) Magnetisation magnitude dependence on composition (controlled by $P_{Ge}/P_{Cr}$) in CrGeTe₃.[113] Reproduced with permission from ref. 113. Copyright 2018 AIP Publishing.

synthesis of atomically thin ferromagnetic FeCl₂ on Au(111) and graphite via molecular beam epitaxy (MBE).[114] The grown material exhibited nanometric grain size and low substrate coverage, enabling only the fabrication of proof-of-concept devices.

Another synthetic strategy that has been utilised to grow 2D magnets is magnetron sputtering, by which thick films of FeCl₂ and FeCl₃ were grown.[115] The technique enables to achieve high coverage in a short time, however, with poor control over the film thickness and ultimately leads to thick films with small grain size and irregular shape. α-RuCl₃, which is a Kitaev antiferromagnet with a low magnetic transition temperature of 7 K in bulk, was synthesised using the vertical Bridgman method.[76] Here RuCl₃ powders were slowly molten in a vertical furnace at 1100 °C and after 80 hours the crystals obtained were large and easy to exfoliate.

Many other members of these family have been predicted to be magnetically active, such as FeX₂[45] and MnX₃,[116] however the experimental demonstration of their synthesis is still missing (to the best of our knowledge). The physical vapour deposition (PVD) growth of NiI₂ has been recently reported by Liu et al. via low pressure sublimation of NiI₂ powders onto SiO₂ or h-BN as target substrate.[117] The growth temperature was set to 450 °C for both substrate materials, however h-BN required only one minute of growth time,

whereas SiO₂ needed 5–10 minutes. Monolayer and few layer flakes were selectively grown only on h-BN with lateral size up to 20 μm, while on SiO₂ the deposited flakes were as thick as 40 nm. Interestingly, other magnetic vdW halides have been synthesised decades ago such as like CoCl₂,[118] GdI₂,[119,120] and FeBr₂[121,122] but no further attempts to grow these materials has been done recently.

### Tellurides

Another important family of magnetic vdW crystals is the binary and ternary metal tellurides. Thus far, to the best of our knowledge, this consists of few materials which have been experimentally demonstrated: FeTe, Fe₃GeTe₂, CrXTe₃ (X = Ge or Si), MnBi₂Te₄, and GdTe₃. However many other tellurides have been recently predicted to show magnetic order, such as ferromagnetic VSnTe₃ and NiSiTe₃.[123] Fe₃GeTe₂ is a metallic ferromagnet in bulk with a Curie temperature of 220 K that drops to 130 K in monolayer form and it presents an Ising-type long range ordering.[91,124] The growth of this material has only been achieved via CVT where ultrapure Fe, Ge, and Te powders were mixed in the 3:1:2 ratio (Fig. 3(c)). The temperature gradient between the powders and the target zone was usually 700–750 °C along with I₂ gas transport agent and the synthesis lasted for several days.[124]
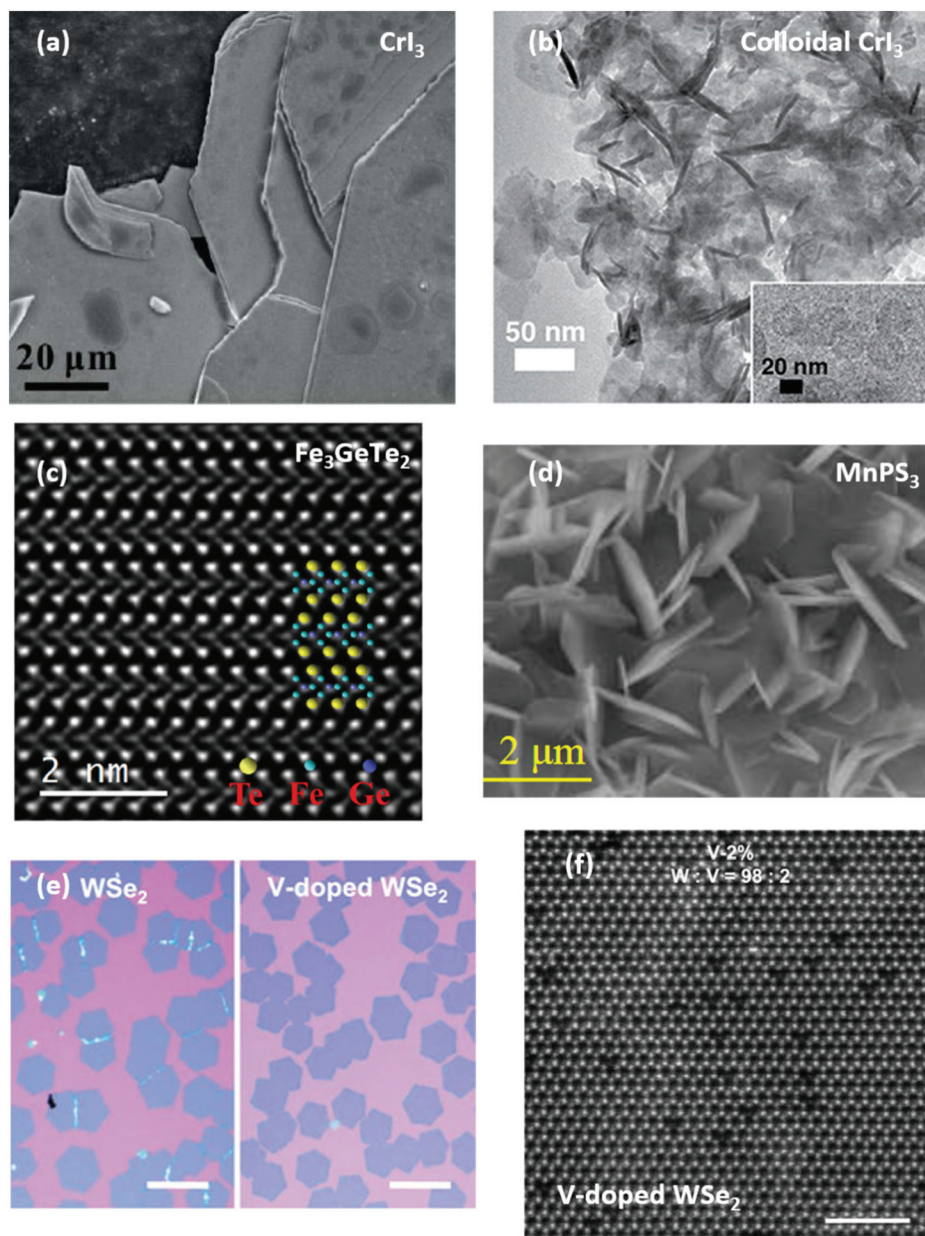
**Fig. 3** Morphology of 2D magnetic crystals. (a) SEM image of a CVT grown CrI$_3$ single crystal.[134] Reproduced with permission from ref. 134. Copyright 2020 Elsevier. (b) Bright field transmission electron microscope (TEM) image of CrI$_3$ colloidal nanocrystals.[110] Reproduced with permission from ref. 110. Copyright 2020 American Chemical Society. (c) High-resolution (HR)TEM of the atomic structure of Fe$_3$GeTe$_2$.[135] Reproduced with permission from ref. 135. Copyright 2019 The American Association for the Advancement of Science. (d) SEM image of CVD-grown MnPS$_3$ microflakes.[136] Reproduced with permission from ref. 136. Copyright 2018 John Wiley and Sons. (e and f) Optical micrographs of CVD-grown undoped WSe$_2$ and V-doped WSe$_2$ alongside HRTEM image showing the presence of dopants.[137] Scale bars are 150 μm and 1 nm. Reproduced with permission from ref. 137. Copyright 2020 John Wiley and Sons.

CrGeTe$_3$ and CrSiTe$_3$ are layered semiconductors and ferromagnetic insulators with Heisenberg and Ising spin order models, respectively.[125,126] Similarly to the other 2D magnets these crystals are expected to present layer dependent magnetic properties, as shown in Fig. 2(b) where the magnetic anisotropy energy increases with the layer number.[111] Both crystals have been grown using a self-flux CVT process, in which Ge or Si and Te powders are loaded in large stoichiometric excess (1 : 3 : 36 molar ration, for example) in an ampoule where they play the role of self-transport agents.[52,126–128] In this case the synthesis can last up to 20 days at temperatures higher than 1000 °C. MBE was used to tune the composition of the Cr–Ge–Te system from Cr$_2$Te$_3$ to CrGeTe$_3$ by varying the relative precursors supply. In this way, it has been possible to tune the magnetic response from a minimum, when Ge was absent, to a maximum where Ge supply was four

times larger than the Cr one, as reported in the plot in Fig. 2(d).[113]

The antiferromagnetic topological insulator $MnBi_2Te_4$ has been also synthesised *via* self-flux CVT over a period of 7 days.[129] This technique has been implemented by mixing the elemental powders in the stoichiometric ratio under vacuum, heating the systems at 850 °C for 24 hours and subsequently at 595 °C for 150 hours. Interestingly, $MnCl_2$ can also be employed as transport agent, if the molar ratio of the three precursors is set at $Mn:Bi:Te:MnCl_2$ 1:1:1:0.3. This different molar ratio has resulted in higher Hall mobilities measured in a magnetoelectronic device. Not only elemental powders can be used, commercial $Bi_2Te_3$ and MnTe bulk powders were employed in the crystal growth and, in addition to this, a complete phase diagram was drawn with Bridgman vertical growth. This has highlighted a plethora of possible phases and stoichiometries.[130,131] These $MnBi_xTe_y$ ($x$ = 2, 4, 6, ...; $y$ = 4, 7, 10, ...) phases have a peculiar structure, where $Bi_2Te_3$ are sandwiched in between two $MnBi_2Te_4$ layers.[112] The separation of $MnBi_2Te_4$ layers has led to the isolation of single 2D ferromagnetic sheets, as represented in Fig. 2(c). Another antiferromagnetic layered material that has been recently reported is $GdTe_3$, which unlike $MnBi_2Te_4$ shows metallic characteristics.[132] The CVT synthesis used Te and Gd powder in a 97:3 ratio, where Te acts as the transport agent, heated at a temperature of 900 °C for 12 hours. Recently, platelets of the 2D ferromagnetic FeTe have been grown *via* ambient-pressure CVD using $FeCl_2$ and Te powder as precursors on $SiO_2$ substrates.[133] In this synthesis, it was possible to selectively grow the tetragonal phase at 530 °C, whereas increasing the growth temperature to 590 °C resulted in the growth of hexagonal crystals. The lateral size of these platelets ranged from 10 to 60 μm with thicknesses down to 2.8 nm.

## Metal phosphochalcogenides

Metal phosphorus trichalcogenides are antiferromagnetic wide band gap semiconductors with general formula $MPX_3$, where M is a metal, or a combination of metals matching the stoichiometry, and X is either S or Se. Specifically two metal atoms coordinate with $[P_2X_6]^{4-}$ ions within the individual layer and arrange into a hexagonal structure. The difference between sulphides and selenides are related to the stacking of the 2D layers in the bulk form, where the firsts are monoclinic ($C2/m$ space group) and the latter are rhombohedral ($R3$ space group).

Besides being magnetically active, these materials attracted research interest due to their catalytic properties and hence more efforts were made towards facile and scalable crystal growth methods.[138,139] CVT is the most used technique to synthesise these bulk crystals (Fig. 4(a)), which also enables to achieve mixed metals phosphochalcogenides such as $CuCrP_2S_6$, $CuInP_2S_6$, and alloys.[140,141] However, He *et al.*
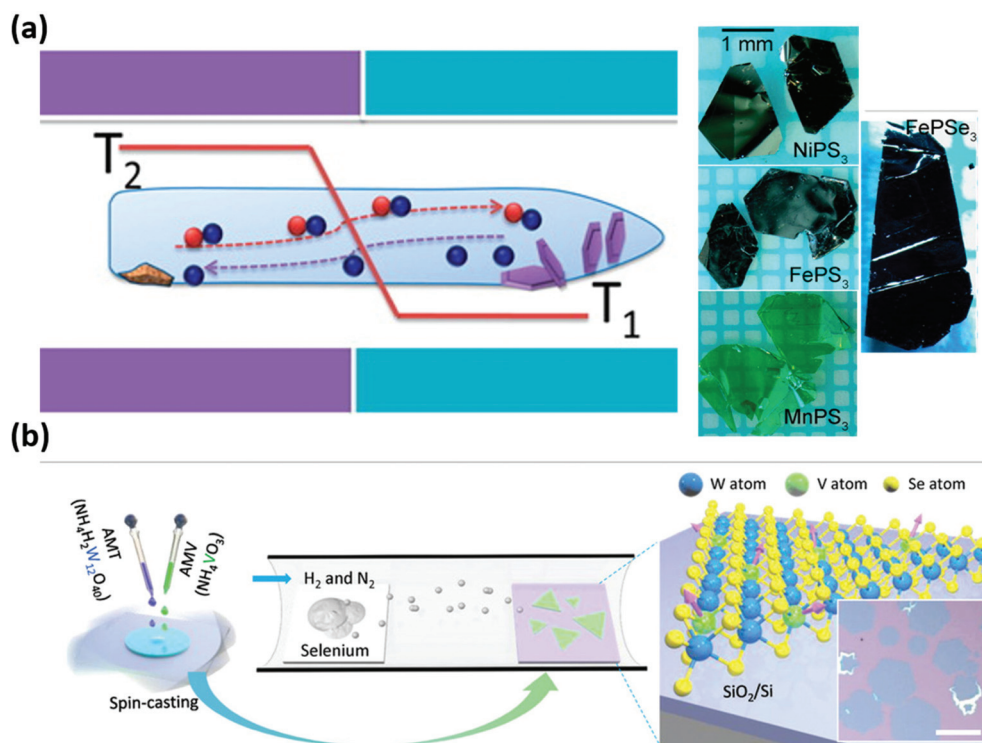


**Fig. 4** Reported growth methods for 2D magnets: CVT and CVD. (a) CVT growth of metal phosphochalcogenides. The sketch depicts the reaction, where the halogen gas transports the elements from the hot to the cold side *via* convection.[146] Reproduced with permission from ref. 146. Copyright 2016 American Chemical Society. (b) CVD of V-doped $WSe_2$. The mixed precursors react with Se on the $SiO_2$ surface into ferromagnetic V-$WSe_2$.[147] Scale bar is 50 μm. Reproduced with permission from ref. 147. Copyright 2020 John Wiley and Sons.

attempted and achieved a higher throughput protocol that involves the hydrothermal synthesis of metal oxides ($NiO_2$ or $MnO_2$) and then a subsequent step in a CVD tubular furnace with stoichiometric quantities of S (Se) and P.[136,142,143] In order to avoid parasitic reactions (formation of metal sulphides), a single phosphosulphide precursor was prepared either by ball milling the powders together or by melting P and S in a pre-growth step. The result was a forest of multilayer $MnPX_3$ (Fig. 3(d)) or $NiPS_3$ with flakes of lateral size around 2–3 μm. While the morphology of such flowers is not suitable for planar device fabrication, this approach proved that it is possible to grow $MPX_3$ crystals *via* CVD. $FePS_3$ has been grown in a similar way, using FeS previously grown on carbon paper and then phosphorised and sulphurised in a tubular furnace at 550 °C.[144] The morphology and dimension of the $FePS_3$ flakes are similar to what has been reported for Ni and Mn based phosphochalcogenides. Huang *et al.* reported analogous results using NaCl crystals as templates, which then are covered in solution with $FeCl_3$ and then placed in a CVD furnace at 500 °C along with P and S powders.[145]

### Transition metal dichalcogenides

Amongst the large family of TMDs the V ($VS_2$, $VSe_2$, $VTe_2$) and Cr ($CrS_2$, $CrSe_2$, $CrTe_2$) compounds are magnetically active, intrinsically or they can become magnetic *via* doping with metal atoms.[81,148–153] These TMDs are mainly antiferromagnetic ($CrS_2$ and $CrSe_2$ are ferromagnets), semimetallic and stable in the 1T trigonal phase (space group $C2/m$) with A–A stacking. CVD-based syntheses of these materials have been demonstrated. Shivayogimath *et al.*[154] have proposed a strategy to achieve a monolayer self-limited synthesis, which is based on the different solubilities of metals and chalcogens in gold recalling the self-limited synthesis of graphene on copper[155] and former growths of group VI TMDs.[156] A thin film of the metal precursor (20 nm) is deposited by PVD on a sapphire substrate and, subsequently, covered with a 500 nm thick gold foil. This composite film is then placed into a hot-wall tubular furnace at high temperature (850 °C) where it is exposed to chalcogen vapours for 10 to 15 minutes. The chalcogen solids are placed upstream and heated at 110 °C, 220 °C, and 420 °C for S, Se, and Te respectively. Since the metal chosen is soluble in gold and the chalcogens have good affinity (decreasing form S to Te) with it, the latter will tend to stick on the Au surface more easily compared to the normally used ceramic substrates ($SiO_2$, sapphire). This facilitates the formation of monolayers that can potentially cover the whole gold surface when adequate reaction time is provided. Using this method, it has been possible to grow flakes of $CrS_2$, $CrSe_2$, $CrTe_2$ and $VS_2$ in addition to many other non-magnetic TMDs. Large $VX_2$ monolayer flakes on $SiO_2$ have been achieved by Liu *et al.*[157] using CVD by salt-assisted (KI) chalcogenisation of $V_2O_5$, a reaction commonly used for group 6 TMDs,[158] at temperatures between 680 to 750 °C in a hot-wall reactor at atmospheric pressure. A similar CVD configuration has been used for the synthesis of multilayered $VTe_2$ nanoflakes by $NH_4Cl$ as evaporation assistant for $V_2O_5$ at temperatures ranging from 600 to 800 °C at atmospheric pressure.[151] Whereas Chua *et al.* reported the CVD growth of $VS_2$ microflowers on carbon paper *via* sulphurisation of $VCl_3$ at just 500 °C at atmospheric pressure set by a mixture 95 : 5 of $Ar/H_2$.[159] $VCl_3$ has also been used along with Te powder in the CVD growth of $VTe_2$ nanoplatelets at a growth temperature of 600 °C, resulting in triangular multilayer flakes up to 10 μm in lateral size.[160]

Magnetism can be induced in other metallic and semiconductive TMDs, such as $MoS_2$, $WSe_2$, $TaS_2$ and $NbS_2$, *via* doping or alloying with a wide range of metal atoms.[84,161–165] However, only few reports have been published showing experimental characterisation of doped-TMDs obtained *via* CVT. Metallic TMDs, such as $TaS_2$ and $NbS_2$ can become magnetically active when layers of metal atoms are intercalated in between the TMDs sheets forming a new crystal structure (space group $P6_322$) with a new stoichiometry of $M_{1/3}Ta(Nb)S_2$. In particular, Cr intercalation in Nb and Ta sulphides yields ferromagnets with $T_c$ at 120 K and 110 K respectively,[166–168] whilst $V_{1/3}NbS_2$ and $V_{1/3}TaS_2$ are almost perfect XY antiferromagnets (spin is out-of-plane by 2°) with much lower Curie temperatures (50 K and 32 K respectively).[169] Fe can also be intercalated in $NbS_2$ resulting in an Ising-nematic antiferromagnet.[83]

Substitutional doping of TMDs has been reported a few times but is yet to be established, and rarely it has been achieved during the CVD growth by adding a third precursor.[170–172] Interestingly, Lee *et al.* have synthesised ferromagnetic monolayer V-doped $WSe_2$ with lateral dimensions of approximately 100 μm onto $SiO_2$ *via* a two-step process.[137,173] Firstly, tungsten and vanadium precursors ($NH_4H_2W_{12}O_4$ and $NH_4VO_3$) are dissolved in deionized water in amount proportionate to the target doping level, then the solution is spin-coated onto a silicon substrate along with NaOH acting as growth promoter. Then, at 750 °C in presence of $H_2$ the metal precursors decompose in metal oxides and react with selenium to form atomically thin V-doped $WSe_2$ monolayers (Fig. 4(b)) extended over tens of microns (Fig. 3(e and f)). A similar synthesis protocol has also been recently used by Pham *et al.* to obtain 10 μm-sized V-doped $WSe_2$ monolayer flakes where larger saturation magnetisations were measured for higher V doping levels up to 8 at%, point in which the distance between the dopant atoms becomes too small to allow ferromagnetism.[174]

# Pathways towards wafer scale synthesis of 2D magnets

CVD is a manufacturing technique which can be upscaled and due to its success in 2D materials synthesis it can be regarded as a promising route for the synthesis of atomically thin 2D magnets over wafer-size areas. Therefore, in this section we will outline the possible pathway towards establishing the (MO)CVD growth of these materials, describing the fundamental physics, possible precursors, process parameters and substrate effects.

## Fundamentals of CVD and MOCVD

After describing the state-of-the-art of 2D magnetic crystals growth, the next step is to identify pathways for the wafer-scale production of these materials and subsequent integration into devices. Looking at the modern electronics industry, most of the materials used for the fabrication of commercial devices require uniform high-quality films with precisely controlled composition to achieve the desired specifications. A technique that conjugates throughput, scalability and precise process control is CVD. Furthermore, CVD can be applied to a wide variety of materials, given the large library of compounds currently employed as precursors for the growth of oxides, semiconductors, nitrides, and metal thin films. The CVD reactor design, related physics, reaction kinetics, and substrate contribution have been extensively investigated for the growth of 2D materials.

After a few years since the isolation of graphene, the CVD synthesis of self-limited monolayer films on a $cm^2$ scale were achieved *via* $H_2$-aided reduction of methane on metal films.[155,175] These results paved the way for the growth atomically thin h-BN and TMDs and similar processing strategies to the ones identified for the graphene synthesis, yielded high quality crystals.[176–178] Up until now, powder precursors have been the nearly only suitable precursors for the growth of high quality atomically thin TMDs due to their reactivity at high temperature and their relative low cost.[179] However, powder-based CVD lacks of a precise control over precursors supply and the growth time is determined by the powder amount, which ultimately limits the coverage and the thickness control. Thus, MOCVD, where the precursors are high vapor pressure solids, liquids, or gases and are individually controlled, has been proposed as a possible solution to these limitations. MOCVD enables control on the precursor flowrates with the possibility to extend the growth time up to several hours. This technique enabled the growth of $MoS_2$, $MoSe_2$, $WS_2$, and $WSe_2$ over more than 2-inch wafers with performances approaching the ones of materials grown using powders.[86,87,180–182]

As we mentioned in the previous section, other bottom-up techniques are used for the growth of 2D materials. We described how MBE can cover a wide range of compositions with high resolution in the Cr–Ge–Te system. Analogous results have also been reported for TMDs,[183,184] where the high degree of process control provided by MBE enabled fundamental studies of nucleation and growth of monolayer $WSe_2$.[185] However, despite the extremely high crystal quality that is achieved, MBE currently leads only to sub micrometric flake sizes with slow deposition rate. Additionally, the technique itself requires extremely pure elemental precursors, high temperatures and ultra-high vacuum in the reaction chamber. Atomic layer deposition (ALD) is less demanding in terms of cost and it can produce large films with controllable thickness.[186] The polycrystalline films with domains normally (within 1–2 μm) much smaller than CVD-grown materials,[187,188] (several microns in lateral size) currently represent the main limitation in using ALD to grow TMDs and it is possibly due to the low deposition temperatures, which are usually around 500 °C.

## The physics of the MOCVD reactors

CVD is a multiscale process, as it involves both macroscopic and microscopic phenomena. The former are: precursor evaporation, reactor fluid dynamics, and heat transport.[189,190] While the latter are: precursors reaction, diffusion, and nucleation and growth.[189] Analogously to liquids flowing in pipes, the physics in a CVD reactor is governed by the Reynolds number *Re*, which determines whether the flow is turbulent or laminar and consequently the fluid dynamics and the precursors distribution.[189] Conventional CVD parameters nearly always result in low *Re* and therefore the process can be modelled using the well-known Navier–Stokes equations, which model the conservation of momentum and mass, and the conservation of heat and chemical species.[191] Solving these equations for the reactor geometry, given specific boundary conditions, results in the temperature, velocity, and concentration profiles across the tube, which are essential information for the process parameter optimisation. To distinguish the individual concentration profiles of all the chemical species, the direct and the inverse reaction rates must be considered, which are usually Arrhenius-like power laws. The solutions of the mass, heat and momentum balance can be included into mesoscale simulations (Kinetic Monte Carlo and phase-field models) as boundary conditions to predict morphology, distribution and size of 2D materials.[192,193] Another key phenomenon to be considered is the formation of the boundary layer where the flow meets the substrate. Within the boundary layer the viscous component of the forces dominate and the gas velocity acquires a component normal to the substrate, inducing a concentration gradient through the layer, as described in Fig. 5(a).[194] Additionally, the boundary layer thickness increases along the substrate by the square root of the *x* coordinate in a horizontal reactor and this causes a drop in the growth rate, ultimately leading to an inhomogeneous film.[195] This is generally mitigated tilting or rotating the substrate to level off the boundary layer contribution,[196,197] however this configuration is rarely present in research labs while it is normally use at industrial level. Therefore, a solution to this issue has been found in using vertical reactors; where the gas flow is normal to the substrate and hence the boundary layer thickness is homogeneous. This ultimately results in a uniform distribution of products (Fig. 5(b)).[198] This configuration proved to be particularly advantageous for MOCVD of TMDs, since J. Robinson, J. Redwing and co-workers have been able to reduce the growth time from the 26 hours, reported for horizontal MOCVD synthesis,[87] to just one hour in a vertical reactor.[199] Moreover, the use of a cold-wall reactor where the substrate is placed onto a graphite susceptor heated by an induction system, which prevents parasitic reactions in the gas phase and minimises the vapour transport led to the synthesis of epitaxial $WSe_2$ monolayer films over large sapphire and h-BN substrates.[199–202]
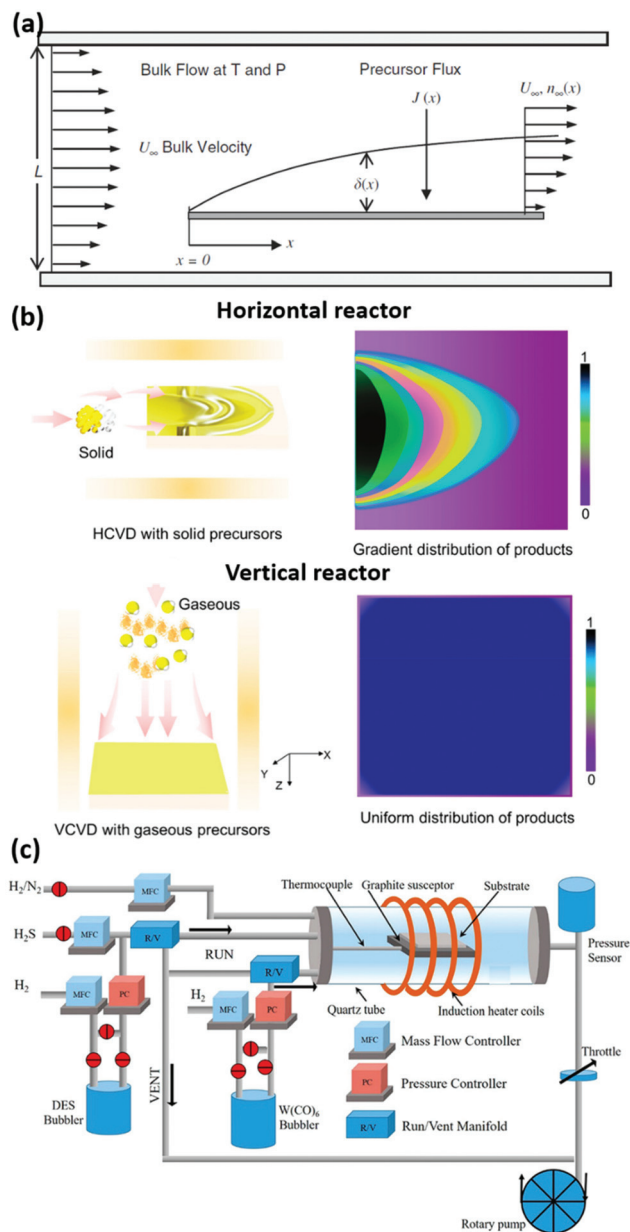
**Fig. 5** Fundamentals of CVD physics and equipment. (a) Sketch of the boundary layer arising in a horizontal furnace. The precursor flux towards the substrate $J(x)$ is a function of the layer thickness $\delta(x)$ and the precursor concentration $n(x)$, both dependent on the horizontal coordinate.[189] Reproduced with permission from ref. 189. Copyright 2008 The Royal Society of Chemistry. (b) Comparison between a conventional horizontal reactor and a vertical reactor. The boundary layer presence results in an inhomogeneous product distribution.[198] Reproduced with permission from ref. 198. Copyright 2020 American Chemical Society. (c) Schematic of a cold-wall CVD reactor for the growth of $WS_2$ from solid ($W(CO)_6$), liquid (diethyl sulphide, DES) or gaseous ($H_2S$) precursors.[203] Reproduced with permission from ref. 203. Copyright 2018 American Chemical Society.

These considerations regarding the flow are of concern of both CVD and MOCVD alike, however the higher degree of precursors flow control in MOCVD makes this technique particu-

larly promising for the growth of 2D materials. In fact, the precursors supply in powder-based CVD cannot be efficiently control as its evaporation rate depends on many factors such as temperature, carrier gas velocity, powder heap height and geometry.[204] Additionally, the precursors amount is limited and therefore does not allow prolonged growth times needed for full coverage on wafer scale. Several strategies to control the precursor flowrates have been proposed, such as using low volatile oxides, to limit the metal precursor evaporation,[205] or mapping the evaporation rate *via* calorimetric analysis,[157] which has improved the crystal quality. On the contrary, in MOCVD the precursors are placed outside the furnace in stainless steel cylindrical bubblers where the carrier gas flows into the cylinders and transport the precursor's vapour in the reactor. The precursor flowrate $F$ is given by $F = \dfrac{p(T)}{P - p(T)}F_{in}$, where $F_{in}$ is the flowrate of the carrier gas, $p(T)$ is the precursor's vapour pressure at the bubbler temperature $T$ and $P$ is the bubbler pressure. Hence, for a robust control of the precursor flowrate a bubbler necessitates to be linked to an upstream mass flow controller (MFC), a pressure controller (PC) downstream and to be placed into a water bath, which controls the temperature and consequently the vapour pressure. If the precursors are compressed gases (*i.e.* hydrides) only a single MFC is required. Such bubblers can be placed in parallel for multi-element compounds, alloying and doping enabling a wide range of compositions in the final product. Alongside the conventional CVD equipment, the precursors used in MOCVD are usually pyrophoric, flammable, or toxic and therefore additional equipment for the effluent treatment is often needed and hazards must be carefully assessed. A good example of a custom-built MOCVD system used for the growth of TMDs is schematically reported in Fig. 5(c).

**Potential precursors for the MOCVD growth of 2D magnets**

The general requirements of MOCVD precursors are: high volatility, high reactivity, stability under atmosphere and possibly low toxicity. However, we can refine these specifications looking at the current state-of-the-art MOCVD growth of TMDs for key parameters and precursors. A key precursor requirement is a low carbon content since it has been shown that organic precursors lead to the deposition of carbonaceous species on the final product.[203,206] This has been partially solved for $WSe_2$ utilising $H_2Se$, which has massively decreased the contamination from carbon and other elements.[86] In addition to this, 2D materials growth needs low precursors flowrates (0.01 sccm for metals and 0.4–5 sccm for chalcogens) unlike classic MOCVD of coatings and thin films where the flowrates are orders of magnitude larger. Thus, it is possible to opt for less volatile precursors when advantageous in terms of safety, availability, and ease of handling.

Looking at the classes of 2D magnets we described earlier, they are formed by: metals (Cr, V, Fe, Mn, Bi, Ni, Ta and Nb), chalcogens (S, Se and Te), halogens (Cl, Br and I), Si, Ge and P. For all these elements there are precursors which are used in CVD industry or research that can be employed for the
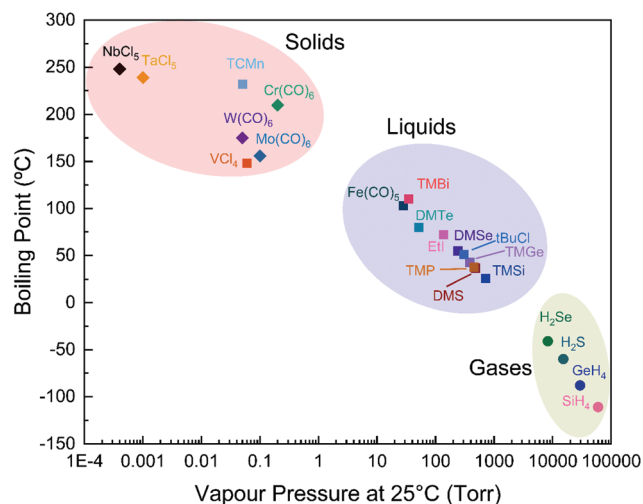
**Fig. 6** Physical properties of the proposed precursors for the (MO)CVD growth of 2D magnets. On the upper-left corner the precursors are in the powder form (VCl$_4$ and TCMn are liquids), in the middle the precursors are liquid and on the lower-right the hydride gases.

growth of 2D magnets. Fig. 6 and Table 2 summarise the physical properties of the proposed precursors.

**Cr-Precursors.** Cr(CO)$_6$ is highly volatile and even more than the currently used molybdenum and tungsten carbonyls (vapour pressures at 25 °C in torr: 0.2 Cr(CO)$_6$, 0.1 Mo(CO)$_6$ and 0.05 W(CO)$_6$)[207] that have been extensively used for MOCVD of MoX$_2$ and WX$_2$. Furthermore, Cr carbonyl has a high pyrolysis rate at temperatures lower than 500 °C enabling the possibility to grow on temperature sensitive substrates.[208] Comparing Cr carbonyl with other Cr-containing commercial MOCVD precursors, it outperforms more complex organochromium molecules in the growth of Cr$_2$O$_3$ at 500 °C achieving the highest growth rate with negligible carbon contamination left.[209]

**V-Precursors.** In the MOCVD growth of VO$_2$ coatings, a wide range of vanadium precursors has been reported,[210] however the most successful compound in terms of phase selectivity and product purity is vanadyl acetylacetonate (VO(acac)$_2$), whose volatility matches the requirements for MOCVD and leaves negligible carbon contamination.[211,212] Another molecule that can potentially be used is VCl$_4$ that has the same vapour pressure of tungsten carbonyl at room temperature. This would be advantageous as $V$ is already in the +4 oxidation state and it does not leave carbon contaminations.[210] However HCl would evolve from the reaction with the chalcogen precursors and hence precautions must be taken.

**Mn-Precursors.** Several organomanganese compounds have been used as dopant source for II–VI semiconductors and in principle can be proposed for the growth of MnBiTe$_4$ and MnPX$_3$.[213] The most widely used is methylcyclopentadienyl–manganese tricarbonyl ((CO)$_3$CH$_3$C$_5$H$_4$Mn, TCMn) despite having the highest cracking temperature of all the class and low volatility.[214,215] As it possesses a vapour pressure compar-

able to the one of W(CO)$_6$ (0.05 torr at 25 °C)[214] at room temperature it may be volatile enough to sustain the growth of atomically-thin materials. Other MOCVD compatible compounds are (C$_5$H$_5$)$_2$Mn, (MeC$_5$H$_4$)$_2$Mn, Me(CO)$_5$Mn and Et(CO)$_5$Mn, which might be more advantageous than TCMn having lower carbon atoms.

**Fe-Precursors.** Another element to cover is iron for the synthesis of FePS$_3$, FePSe$_3$, and Fe$_3$GeTe$_2$. Iron pentacarbonyl (Fe(CO)$_5$) and ferrocene (FeC$_{10}$H$_{10}$) are low in carbon content and they have been established in the MOCVD growth of Fe, FeS$_2$ and Fe$_2$O$_3$.[216–218] Iron pentacarbonyl could be better suitable since it has lower carbon content and a lower cracking temperature of 300 °C than ferrocene.[219,220]

**Ni-Precursors.** Similarly, Ni(CO)$_4$ can potentially be used as Ni-precursor since it has been employed for the growth of Ni thin films at low temperature (175–400 °C), due to its extremely high volatility and low cracking temperature of ~200 °C.[221] However, it presents acute toxicity and hence, alternative nickelorganic precursors have also been reported.[222] Nickel pentacene (Ni(C$_5$H$_5$)$_2$) and Ni(dmg)$_2$ (nickel bis(dimethylglyoxime)) proved to be efficient to yield Ni films of high quality with a negligible amount of impurities.[223–225]

**Bi-Precursors.** The perfect example of a Bi-based material to look at is Bi$_2$Te$_3$, as it is a vdW crystal and it is widely produced *via* MOCVD. The typical MOCVD growth is based on the reaction between trimethyl bismuth (TMBi) and an organotelluride that can be diethyl telluride (DETe) or di-isopropyl telluride (DiPTe) at the moderate temperature of ~450 °C.[226–228] Most of the Bi$_2$Te$_3$ produced is in the form of films of hundreds of nm in thickness using precursors flowrate several order of magnitudes larger than values reported for TMDs. Bi$_2$Te$_3$ in the monolayer or few-layered form has not been reported yet.

**Nb–Ta-precursors.** Several organometallic compounds are widely used for the growth of Nb and Ta nitrides and oxides, (such as Ta(NCMe$_3$)(NEtMe)$_3$ or Nb(N$^t$Bu)(NMe$_2$){C(N$^i$Pr)$_2$(NMe$_2$)}$_2$) however these are large molecules with a high number of carbon atoms and functional groups.[229–233] Therefore, precursors more suitable for the growth of 2D NbX$_2$ and TaX$_2$ could be carbon-free molecules such as NbCl$_5$ and TaCl$_5$. These two precursors both possess high vapour pressures[234] and have already been used for the growth of atomically-thin sulphides by reaction with sulphur powder at high temperature.[235–237] Additionally, a solid example of the use of NbCl$_5$ in MOCVD has been reported by Kozhakhmetov *et al.* where few layered 3R-NbS$_2$ was obtained using gaseous H$_2$S and H$_2$ as carrier gas.[182]

**S, Se, Te-precursors.** Chalcogen precursors for 2D materials have been extensively explored in MOCVD of group VI sulphides and selenides. The most used one are organochalcogens, which are formed by two alkyl tails of length ranging from one to three carbon atoms bonded with a chalcogen atom. In particular diethyl sulphide (DES) has been used in almost all of the MOCVD reports of MoS$_2$ and WS$_2$ achieving full coverage of monolayers on both sapphire and amorphous silica, showing good optical and electronic transport properties despite the submicrometric grain size.[87,238] It is poss-

**Table 2** Vapour pressure laws, melting and boiling point of potential precursors

| Precursor | Melting point (°C) | Boiling point (°C) | $\text{Log}(P_{vapour}, \text{torr})$ |
|---|---|---|---|
| **Group V** | | | |
| $VCl_4$ | −25 | 148 | 0.06 at 298 K (ref. 265) |
| $NbCl_5$ | 205 | 248 | $17.263 - 4732/T - 0.7912\ln(T) - 29263/T^2$ (ref. 234) |
| $TaCl_5$ | 216 | 239 | $21.199 - 4831/T - 1.399\ln(T) - 7648/T^2$ (ref. 234) |
| **Group VI** | | | |
| $Cr(CO)_6$ | 90 | 210 | $11.475 - 3622.9/T$ [207] |
| $Mo(CO)_6$ | 150 | 156 | $11.7274 - 3788.3/T$ [207] |
| $W(CO)_6$ | 170 | 175 | $10.947 - 3640.4/T$ [207] |
| **Group VII** | | | |
| TCMn | −1 | 232 | 0.05 at 298 K (ref. 266) |
| **Group VIII** | | | |
| $Fe(CO)_5$ | −21 | 103 | $8.073 - 1960.869/(T - 0.228)$ [267] |
| $Fe(C_5H_5)_2$ | 173 | 249 | |
| **Group X** | | | |
| $Ni(CO)_4$ | −17 | 43 | $7.512 - 1409.037/(T - 11.637)$ [267] |
| $Ni(C_5H_5)_2$ | 171 | | $2.124 - 3651.114/T$ [268] |
| **Group XIV** | | | |
| $SiH_4$ | −185 | −112 | $7.097 - 703.987/(T + 5.352)$ [267] |
| TMSi | −99 | 26 | $6.852 - 1047.272/(T - 36.057)$ [269] |
| $SiCl_4$ | −69 | 58 | $7.704 - 1616.546/(T + 5.305)$ [270] |
| $GeH_4$ | −165 | −88 | $6.981 - 736.692/(T - 4.665)$ [267] |
| TMGe | −88 | 43 | $6.986 - 1166.492/(T - 33.005)$ [267] |
| $GeCl_4$ | −50 | 87 | $6.557 - 1080.101/(T - 63.588)$ [267] |
| **Group XV** | | | |
| P (red) | | 590 (sublimates) | $7.917 - 2819.239/(T + 6.399)$ [267] |
| $PH_3$ | −133 | −88 | $6.9 - 702.651/(T - 11.065)$ [267] |
| TMP | −86 | 38 | $7.7329 - 1512/T$ [257] |
| TEP | | 127 | $7.86 - 2000/T$ [257] |
| TMBi | −86 | 110 | $6.984 - 1388.9/(T - 42.374)$ [271] |
| **Group XVI** | | | |
| S | 115 | 445 | $91.489 - 8170/T - 12.61\ln(T) + 0.0035T$ [272] |
| $H_2S$ | −82 | −60 | $7.403 - 958.587/(T - 0.539)$ [267] |
| DMS | −98 | 36 | $7.162 - 1201.134/(T - 29.906)$ [273] |
| DES | −104 | 92 | $7.541 - 1560.523/(T - 26.557)$ [267] |
| Se | 221 | 685 | $8.0886 - 4989/T$ [274] |
| $H_2Se$ | −66 | −41 | $6.492 - 596.484(T - 66.353)$ [267] |
| DMSe | −87 | 55 | $7.696 - 1665.9/T$ [275] |
| $DMSe_2$ | | 156 | $13.585 - 3912.8/T$ [275] |
| Te | 450 | 988 | $7.5999 - 5906.2/T$ [274] |
| DMTe | −10 | 82 | $7.97 - 1865/T$ [257] |
| DETe | | 137 | $7.99 - 2093/T$ [257] |
| DiPTe | | 49 | $8.288 - 2309/T$ [276] |
| **Group XVII** | | | |
| tBuCl | −26 | 51 | $7.129 - 1281.242/(T - 21.795)$ [267] |
| nHexCl | −94 | 133 | $6.769 - 1304.968/(T - 73.092)$ [277] |
| EtI | −111 | 72 | $6.96 - 1247.135/(T - 39.612)$ [267] |

ible to use dimethyl sulfide to reduce the carbon incorporation as shown by Shinde *et al.* however its extremely high volatility may reduce the flowrate control.[180] Di-*tert*-butyl sulphide has also been reported as precursor for $MoS_2$, however the high number of carbon atoms resulted in carbon contamination specifically at high pressure and temperature.[239,240] Analogously, dimethyl selenide (DMSe) proved to be a suitable precursor for $MoSe_2$ and $WSe_2$ owing to its lower volatility compared to DMS and therefore easier to control.[241,242] In order to prevent the carbon contamination, it is possible to switch to hydrides ($H_2S$ and $H_2Se$), however these compounds are extremely toxic and it might be challenging their use in university research laboratories, posing also concerns over the scalability of the synthesis.[203,206] As no atomically-thin telluride has been reported *via* MOCVD yet, therefore to propose a suitable precursor for future synthesis of binary and ternary magnetic telluride we have to look at the production of non-layered semiconductors. The perfect example is the epitaxial growth of HgCdTe, a small band gap semiconductor used for infra-red detection. This material is the result of a solid solution between HgTe and CdTe, whose bandgap can be tuned by varying the Hg/Cd ratio during growth.[243] Such a fine tuning has been achieved *via* MOCVD adjusting the flowrates of mercury vapours and dimethyl cadmium (DMCd) using GaAs, Si or sapphire as epitaxial substrates.[244] The metal precursors react with dimethyl telluride (DMTe) and hydrogen to form $Hg_xCd_{1-x}Te$ at a temperature of 400 °C, which is much lower than the temperatures used for liquid phase growth techniques.[245] Similarly, CdZnTe can be grown using similar precursors and temperature starting from diethylzinc (DEZn).[246] Interestingly, the low growth temperature allows to control the rate limiting step of the process, since at $T < 430$ °C the reac-

tion is kinetically-driven and the activation energy determines the final composition whereas for higher temperature the limiting step is the mass transport and the diffusivity of each element.[247]

**Si–Ge precursors.** Similarly to chalcogens, silicon and germanium hydrides are established gaseous carbon-free precursors. In fact, $SiH_4$ and $GeH_4$ are both used for epitaxial growth of Si and Ge films and Si-doping of GaAs and they possess moderate cracking temperature in presence of $H_2$ as carrier gas (~600 °C for $GeH_4$).[248–252] However, they are both pyrophoric and extremely toxic. Both tetramethyl silane and germane have been reported as suitable MOCVD precursors being highly volatile and much less toxic than hydrides.[253–255] Furthermore, $SiCl_4$ and $GeCl_4$ have low toxicity and they are C-free precursors often used in epitaxial growth of Ge, $GeO_2$ and $SiO_2$ growth.[255,256]

**P-Precursors.** For the growth of metal phosphochalcogenides, we listed the potential precursors for metals, sulphur and selenium, therefore we discuss possible precursors for P, proposing alternatives to the extremely toxic phosphine gas ($PH_3$). Trimethyl and triethyl phosphine (($CH_3$)$_3$P TMP, ($CH_3CH_2$)$_3$P TEP), are highly volatile at room temperature (VP: 493 torr for TMP, 15 torr for TEP) and their toxicity level is lower than the phosphine one, thus they could be available option.[257] Their use has already been tested in the MOCVD growth of InP and as P-dopants sources in n-type diamond, without any difference in quality compared to the use of $PH_3$.[258–261]

**Halogen precursors.** Very few precursors are reported in the literature since most of the metal halides are synthesized *via* CVT where gaseous chlorine, iodine and bromine are used. Potential Cl precursors were tested by Barrioz *et al.* in the MOCVD growth of $CdCl_2$ on CdTe films, *tert*-butyl chloride (*t*BuCl) and *n*-hexyil chloride (*n*-HexCl) reacted with DMCd at temperatures ranging from 350 to 450 °C.[262] The best result was achieved with *t*BuCl at 400 °C since *n*-HexCl did not efficiently crack at the explored temperatures. Similarly, the only iodine MOCVD precursor reported in the literature is iodoethane ($CH_3CH_2I$, ethyl iodide), which has a vapour pressure of 100 torr at room temperature and it has been employed as I-dopant source for ZnS and Cu films.[263,264] Unfortunately, bromine is yet to be reported as element in a CVD process, therefore, in analogy with the I-precursor, we propose bromoethane as potential precursor. Alternatively, it may be possible to use halogen gases directly in the MOCVD process analogously to oxygen and hydrogen, widely used as reagents or reducing/oxidant agents.

## The role of the growth substrate

The substrate choice is a fundamental parameter in the CVD process since crystal structure, morphology and high temperature stability of the substrate material directly influence the growth kinetics. These aspects have been extensively discussed in recent reviews.[179,278,279] For 2D materials in particular, the interactions between film and substrate determine not only the morphology of the grown layer but also nuclei density, optical properties, strain and crystal phase. We can divide the substrates into chemically inert *versus* chemically reactive. The most prominent example of this second category is Cu for the growth of graphene that acts as a catalyst for methane cracking reaction combined with the poor C solubility.[280] Similarly, h-BN growth is catalysed by iron that additionally acts as nitrogen reservoir when preannealed with ammonia, enabling in this way full coverage.[281,282] Au foil plays a similar role for TMDs where the limited solubility of chalcogens confines the growth to the first layer resulting in large area monolayers.[283–285]

Regarding chemically inert substrates, the most used one is $SiO_2$/Si as it is inexpensive and technologically relevant for electronic devices and it enables a stark optical contrast between the flakes and the substrate. Numerous examples of large isolated TMDs flakes have been reported in the literature using powder CVD,[290,291] whereas full coverage has been achieved *via* MOCVD.[87,180] However, the roughness of the silica combined with the difference in thermal expansion coefficient compared with TMDs induces in the flake a consistent strain, which is detrimental for the optical properties of the grown material.[292,293] Moreover, the orientation of the flakes is completely random and therefore when coalescing the film presents a high concentration of grain boundaries, which is detrimental for the charge carrier mobilities. Substituting amorphous $SiO_2$ with crystalline substrates, such as sapphire, h-BN (Fig. 7(a)) or $SrTiO_3$, it is possible to govern the domain orientation and minimise the antiphase boundaries.[202,294,295] Additionally the vdW surface of 2D materials prevents the bonding between the film and the substrate avoiding possible lattice mismatches and therefore the presence of strain. It is also possible to engineer the nucleation *via* spincoating organic compounds (perylene-3,4,9,10-tetracarboxylic acid tetrapotassium salt, PTAS the most common)[287] that lower the nucleation energy barrier and act as nucleation promoters, as reported in Fig. 7(c and d). In this way, it has been demonstrated the possibility of CVD of $MoS_2$ over large area at a lower temperature ~650 °C compared to conventional powder CVD.[296] The substrate crystal lattice can also be used to select the phase of 2D materials in case of polymorphism. A notable example is the lattice restructuring of orthorhombic SnS into 1T-$SnS_2$ onto monolayer $WS_2$ that act as templating substrate and that has the advantage of a dangling bond-free and clean interface as represented in Fig. 7(b)[286] Similarly, 2D γ-InSe can be grown selectively from other layered stoichiometries and phases by vapor transport starting from InSe powder.[297] Applying a moderate temperature gradient (500–600 °C) on the template substrate, which is mechanically exfoliated ε-GaSe, the separation of the desired γ-InSe in the coldest zone and the $In_2Se_3$ polytypes in the hottest one is achieved. Another notable example is the growth of the non-vdW ferromagnetic $Cr_2S_3$, because Cr exists also in +3 oxidation state and it forms rhombohedral $Cr_2S_3$ as well as 1T-$CrS_2$.[298,299] In particular, the former was achieved by using atomically smooth fluorophlogopite mica since $SiO_2$ yielded mixed phases and an irregular morphology.[300,301]
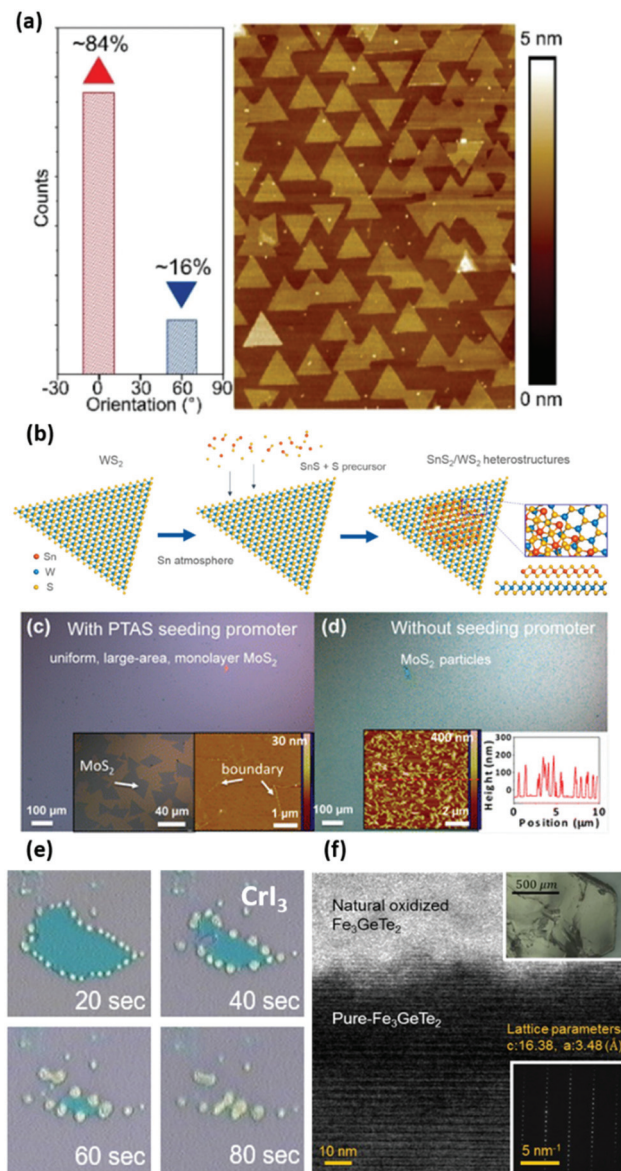
**Fig. 7** Substrate and environment influence on 2D materials. (a) Atomic force microscopy (AFM) map of highly-oriented $WSe_2$ grown *via* MOCVD on h-BN and relative orientation count.[202] Reproduced with permission from ref. 202. Copyright 2019 American Chemical Society. (b) Schematic that shows a $WS_2$ flake that templates the growth of layered $SnS_2$ from SnS and S precursors.[286] Reproduced with permission from ref. 286. Copyright 2019 American Chemical Society. (c and d) Optical images and AFM maps of $MoS_2$ crystals grown with and without the nucleation promoter PTAS.[287] Reproduced with permission from ref. 287. Copyright 2014 American Chemical Society. (e) Extremely fast degradation of fewlayered $CrI_3$ under atmosphere and focused light.[288] Reproduced with permission from ref. 288. Copyright 2018 American Chemical Society. (f) HRTEM micrograph that reports the visibly thick oxide layer on multilayer $Fe_3GeTe_2$.[289] Reproduced with permission from ref. 289. Copyright 2019 IOP Publishing.

### Encapsulation of 2D magnetic materials

A shared issue for the whole 2D materials is the degradation under atmosphere *via* reaction with oxygen and moisture.[302]

Oxidation in atomically thin crystals has been demonstrated to be extremely detrimental for optical and electronic properties and poses an additional challenge for the future device integration.[303–305] 2D tellurides ($MoTe_2$ and $WTe_2$) are particularly sensitive to the environmental conditions where Te converts into Te oxides after few hours after the synthesis.[306–308] Similar phenomena has also been observed in 2D magnetically active tellurides $CrSi(Ge)Te_3$ [309] and $Fe_3GeTe_2$, whose oxidation led to poorer magnetic properties in a multilayer sample (Fig. 7(f)).[289] $CrI_3$ undergoes an even more severe degradation process, which is catalysed by ambient light and dissolves exfoliated crystals in a few minutes as seen in Fig. 7(e).[288] Several possible strategies to overcome this important limitations have been proposed, such as coating with polymers or encapsulating with air-stable thin films.[310] The encapsulation with h-BN layers has proved to be a successful strategy for protecting 2D materials, which also enables to improve charge carrier mobilities[311] and light emission properties in $MoS_2$.[312,313] Regarding the synthesis of h-BN, several MOCVD papers have reported the large-scale growth of mono- and fewlayers over different metallic and inert substrates.[314–317] Therefore, after the first growth of the desired 2D magnet it may be possible to directly deposit a protective layer of h-BN by switching precursors and parameters in the same reactor. Additionally, the use of glove boxes connected with the MOCVD chamber would enable to preserve air and moisture sensitive material and to deposit protective capping layer of different nature using different deposition techniques.

## Conclusions and outlook

van der Waals materials with magnetic ordering holds tremendous interest for fundamental physics investigation and novel device fabrication. Progress has been made in the understanding of their fundamental properties and device demonstration is at the early stages. We have described how pioneering work have been based on exfoliated materials to understand magnetism and spin dynamics in 2D. We have emphasised how materials grown in mono and few-layered form extended over large areas will not only allow the systematic study of their properties but will also enable the direct integration in van der Waals heterostructures for the fabrication of functional devices. The integration of 2D magnets grown by CVD in functional spintronics heterostructures can be foreseen to serve to the emerging field of spintronics circuits. As the use of CVD synthesis has revolutionised the investigation of graphene, similarly MOCVD is enabling the advancement of 2D TMDs devices. We envision that the wide range of 2D magnets can also see a similar progress once MOCVD enables the achievement of large area atomically thin films. Here we have reviewed the state of the art of the synthesis of metal halides, binary and ternary metal tellurides, doped TMDs, and metal phosphochalcogenides. We have highlighted that CVT is the predominant available synthesis route, which leads to the formation of high-quality bulk crystals that then require to be microme-

chanically exfoliated to be studied in the atomically thin form. The only 2D magnetic materials that have been CVD grown in the atomically thin form are V and Cr-based TMDs as well as doped-TMDs. We have then identified potential precursors for the main classes of 2D magnetic materials, and we have critically discussed their suitability for the MOCVD synthesis on the bases of their physical properties, research and industrial usage and safety. In specific, the precursor volatility is critical as highly volatile compounds enable an efficient supply with robust control. More efforts in this synthesis technique will be required to see the field moving towards the construction of different device architecture and materials assembly to explore the potential of spintronic circuits. We believe that the establishment of a new platform for vdW atomically thin and magnetically ordered materials synthesis will provide exciting opportunities for future data storage and communication devices.

## Conflicts of interest

The authors declare no conflicts of interest.

## Acknowledgements

## References

1 C. Chappert, A. Fert and F. N. Van Dau, *Nat. Mater.*, 2007, **6**, 813–823.

2 A. V. Khvalkovskiy, D. Apalkov, S. Watts, R. Chepulskii, R. S. Beach, A. Ong, X. Tang, A. Driskill-Smith, W. H. Butler, P. B. Visscher, D. Lottis, E. Chen, V. Nikitin and M. Krounbi, *J. Phys. D: Appl. Phys.*, 2013, **46**, 74001.

3 S. Bhatti, R. Sbiaa, A. Hirohata, H. Ohno, S. Fukami and S. N. Piramanayagam, *Mater. Today*, 2017, **20**, 530–548.

4 Y. Liu and G. Yu, *Nat. Electron.*, 2019, **2**, 555–556.

5 B. Dieny, I. L. Prejbeanu, K. Garello, P. Gambardella, P. Freitas, R. Lehndorff, W. Raberg, U. Ebels, S. O. Demokritov, J. Akerman, A. Deac, P. Pirro, C. Adelmann, A. Anane, A. V. Chumak, A. Hirohata, S. Mangin, S. O. Valenzuela, M. C. Onbaşlı, M. d'Aquino, G. Prenat, G. Finocchio, L. Lopez-Diaz, R. Chantrell,

O. Chubykalo-Fesenko and P. Bortolotti, *Nat. Electron.*, 2020, **3**, 446–459.

6 B. Behin-Aein, D. Datta, S. Salahuddin and S. Datta, *Nat. Nanotechnol.*, 2010, **5**, 266–270.

7 S. Manipatruni, D. E. Nikonov, C. C. Lin, T. A. Gosavi, H. Liu, B. Prasad, Y. L. Huang, E. Bonturim, R. Ramesh and I. A. Young, *Nature*, 2019, **565**, 35–42.

8 D. D. Awschalom, L. C. Bassett, A. S. Dzurak, E. L. Hu and J. R. Petta, *Science*, 2013, **339**, 1174–1179.

9 J. Torrejon, M. Riou, F. A. Araujo, S. Tsunegi, G. Khalsa, D. Querlioz, P. Bortolotti, V. Cros, K. Yakushiji, A. Fukushima, H. Kubota, S. Yuasa, M. D. Stiles and J. Grollier, *Nature*, 2017, **547**, 428–431.

10 W. A. Borders, A. Z. Pervaiz, S. Fukami, K. Y. Camsari, H. Ohno and S. Datta, *Nature*, 2019, **573**, 390–393.

11 J. Grollier, D. Querlioz, K. Y. Camsari, K. Everschor-Sitte, S. Fukami and M. D. Stiles, *Nat. Electron.*, 2020, **3**, 360–370.

12 M. Yang, Y. Deng, Z. Wu, K. Cai, K. W. Edmonds, Y. Li, Y. Sheng, S. Wang, Y. Cui, J. Luo, Y. Ji, H. Z. Zheng and K. Wang, *IEEE Electron Device Lett.*, 2019, **40**, 1554–1557.

13 K. Cai, M. Yang, H. Ju, S. Wang, Y. Ji, B. Li, K. W. Edmonds, Y. Sheng, B. Zhang, N. Zhang, S. Liu, H. Zheng and K. Wang, *Nat. Mater.*, 2017, **16**, 712–716.

14 Y. Cao, A. Rushforth, Y. Sheng, H. Zheng and K. Wang, *Adv. Funct. Mater.*, 2019, **29**, 1808104.

15 P. Seneor, B. Dlubak, M. B. Martin, A. Anane, H. Jaffres and A. Fert, *MRS Bull.*, 2012, **37**, 1245–1254.

16 S. Roche, J. Åkerman, B. Beschoten, J. C. Charlier, M. Chshiev, S. P. Dash, B. Dlubak, J. Fabian, A. Fert, M. Guimarães, F. Guinea, I. Grigorieva, C. Schönenberger, P. Seneor, C. Stampfer, S. O. Valenzuela, X. Waintal and B. Van Wees, *2D Mater.*, 2015, **2**, 030202.

17 M. Piquemal-Banci, R. Galceran, M.-B. Martin, F. Godel, A. Anane, F. Petroff, B. Dlubak and P. Seneor, *J. Phys. D: Appl. Phys.*, 2017, **50**, 203002.

18 V. M. Karpan, G. Giovannetti, P. A. Khomyakov, M. Talanana, A. A. Starikov, M. Zwierzycki, J. Van Den Brink, G. Brocks and P. J. Kelly, *Phys. Rev. Lett.*, 2007, **99**, 176602.

19 B. Dlubak, M. B. Martin, R. S. Weatherup, H. Yang, C. Deranlot, R. Blume, R. Schloegl, A. Fert, A. Anane, S. Hofmann, P. Seneor and J. Robertson, *ACS Nano*, 2012, **6**, 10930–10934.

20 W. Lv, Z. Jia, B. Wang, Y. Lu, X. Luo, B. Zhang, Z. Zeng and Z. Liu, *ACS Appl. Mater. Interfaces*, 2018, **10**, 2843–2849.

21 M. Piquemal-Banci, R. Galceran, F. Godel, S. Caneva, M. B. Martin, R. S. Weatherup, P. R. Kidambi, K. Bouzehouane, S. Xavier, A. Anane, F. Petroff, A. Fert, S. M. M. Dubois, J. C. Charlier, J. Robertson, S. Hofmann, B. Dlubak and P. Seneor, *ACS Nano*, 2018, **12**, 4712–4718.

22 P. U. Asshoff, J. L. Sambricio, S. Slizovskiy, A. P. Rooney, T. Taniguchi, K. Watanabe, S. J. Haigh, V. Fal'Ko, I. V. Grigorieva and I. J. Vera-Marun, *Nano Lett.*, 2018, **18**, 6954–6960.

23 C. K. Safeer, J. Ingla-Aynés, F. Herling, J. H. Garcia, M. Vila, N. Ontoso, M. R. Calvo, S. Roche, L. E. Hueso and F. Casanova, *Nano Lett.*, 2019, **19**(2), 1074–1082.

24 T. Wakamura, F. Reale, P. Palczynski, S. Guéron, C. Mattevi and H. Bouchiat, *Phys. Rev. Lett.*, 2018, **120**, 106802.

25 T. Wakamura, F. Reale, P. Palczynski, M. Q. Zhao, A. T. C. Johnson, S. Guéron, C. Mattevi, A. Ouerghi and H. Bouchiat, *Phys. Rev. B*, 2019, **99**, 245402.

26 J. J. Chen, J. Meng, Y. B. Zhou, H. C. Wu, Y. Q. Bie, Z. M. Liao and D. P. Yu, *Nat. Commun.*, 2013, **4**, 1–7.

27 N. Zibouche, A. Kuc, J. Musfeldt and T. Heine, *Ann. Phys.*, 2014, **526**, 395–401.

28 M. B. Martin, B. Dlubak, R. S. Weatherup, H. Yang, C. Deranlot, K. Bouzehouane, F. Petroff, A. Anane, S. Hofmann, J. Robertson, A. Fert and P. Seneor, *ACS Nano*, 2014, **8**, 7890–7895.

29 F. Godel, M. Venkata Kamalakar, B. Doudin, Y. Henry, D. Halley and J. F. Dayen, *Appl. Phys. Lett.*, 2014, **105**, 152407.

30 A. Manchon, H. C. Koo, J. Nitta, S. M. Frolov and R. A. Duine, *Nat. Mater.*, 2015, **14**, 871–882.

31 H. Yang, A. D. Vu, A. Hallal, N. Rougemaille, J. Coraux, G. Chen, A. K. Schmid and M. Chshiev, *Nano Lett.*, 2016, **16**, 145–151.

32 E. D. Cobas, O. M. J. Van 'T Erve, S. F. Cheng, J. C. Culbertson, G. G. Jernigan, K. Bussman and B. T. Jonker, *ACS Nano*, 2016, **10**, 10357–10365.

33 H. Yang, G. Chen, A. A. C. Cotta, A. T. N'DIaye, S. A. Nikolaev, E. A. Soares, W. A. A. MacEdo, K. Liu, A. K. Schmid, A. Fert and M. Chshiev, *Nat. Mater.*, 2018, **17**, 605–609.

34 Q. Shao, G. Yu, Y. W. Lan, Y. Shi, M. Y. Li, C. Zheng, X. Zhu, L. J. Li, P. K. Amiri and K. L. Wang, *Nano Lett.*, 2016, **16**, 7514–7520.

35 I. A. Verzhbitskiy, H. Kurebayashi, H. Cheng, J. Zhou, S. Khan, Y. P. Feng and G. Eda, *Nat. Electron.*, 2020, **3**, 460–465.

36 M. Z. Iqbal, M. W. Iqbal, S. Siddique, M. F. Khan and S. M. Ramay, *Sci. Rep.*, 2016, **6**, 1–6.

37 A. Dankert, P. Pashaei, M. V. Kamalakar, A. P. S. Gaur, S. Sahoo, I. Rungger, A. Narayan, K. Dolui, M. A. Hoque, R. S. Patel, M. P. De Jong, R. S. Katiyar, S. Sanvito and S. P. Dash, *ACS Nano*, 2017, **11**, 6389–6395.

38 M. Galbiati, S. Tatay, S. M. M. Dubois, F. Godel, R. Galceran, S. Mañas-Valero, M. Piquemal-Banci, A. Vecchiola, J. C. Charlier, A. Forment-Aliaga, E. Coronado, B. Dlubak and P. Seneor, *Phys. Rev. Appl.*, 2019, **12**, 44022.

39 V. Zatko, M. Galbiati, S. M.-M. Dubois, M. Och, P. Palczynski, C. Mattevi, P. Brus, O. Bezencenet, M.-B. Martin, B. Servet, J.-C. Charlier, F. Godel, A. Vecchiola, K. Bouzehouane, S. Collin, F. Petroff, B. Dlubak and P. Seneor, *ACS Nano*, 2019, **13**(12), 14468–14476.

40 T. M. G. Mohiuddin, E. Hill, D. Elias, A. Zhukov, K. Novoselov and A. Geim, *IEEE Trans. Magn.*, 2008, **44**(11), 2624–2627.

41 T. Song, X. Cai, M. W. Y. Tu, X. Zhang, B. Huang, N. P. Wilson, K. L. Seyler, L. Zhu, T. Taniguchi, K. Watanabe, M. A. McGuire, D. H. Cobden, D. Xiao, W. Yao and X. Xu, *Science*, 2018, **360**, 1214–1218.

42 D. R. Klein, D. MacNeill, J. L. Lado, D. Soriano, E. Navarro-Moratalla, K. Watanabe, T. Taniguchi, S. Manni, P. Canfield, J. Fernández-Rossier and P. Jarillo-Herrero, *Science*, 2018, **360**, 1218–1222.

43 W. Zhang, P. K. J. Wong, R. Zhu and A. T. S. Wee, *InfoMat*, 2019, **1**, 479–495.

44 H. Lin, F. Yan, C. Hu, Q. Lv, W. Zhu, Z. Wang, Z. Wei, K. Chang and K. Wang, *ACS Appl. Mater. Interfaces*, 2020, **12**(39), 43921–43926.

45 M. Ashton, D. Gluhovic, S. B. Sinnott, J. Guo, D. A. Stewart and R. G. Hennig, *Nano Lett.*, 2017, **17**, 5251–5257.

46 S. J. Gong, C. Gong, Y. Y. Sun, W. Y. Tong, C. G. Duan, J. H. Chu and X. Zhang, *Proc. Natl. Acad. Sci. U. S. A.*, 2018, **115**, 8511–8516.

47 F. Casper, T. Graf, S. Chadov, B. Balke and C. Felser, *Semicond. Sci. Technol.*, 2012, **27**, 063001.

48 Y. Cao, Y. Sheng, K. W. Edmonds, Y. Ji, H. Zheng and K. Wang, *Adv. Mater.*, 2020, **32**, 1907929.

49 D. L. Cortie, G. L. Causer, K. C. Rule, H. Fritzsche, W. Kreuzpaintner and F. Klose, *Adv. Funct. Mater.*, 2020, **30**, 1901414.

50 C. Gong, L. Li, Z. Li, H. Ji, A. Stern, Y. Xia, T. Cao, W. Bao, C. Wang, Y. Wang, Z. Q. Qiu, R. J. Cava, S. G. Louie, J. Xia and X. Zhang, *Nature*, 2017, **546**, 265–269.

51 B. Huang, G. Clark, E. Navarro-Moratalla, D. R. Klein, R. Cheng, K. L. Seyler, D. Zhong, E. Schmidgall, M. A. McGuire, D. H. Cobden, W. Yao, D. Xiao, P. Jarillo-Herrero and X. Xu, *Nature*, 2017, **546**, 270–273.

52 V. Carteaux, D. Brunet, G. Ouvrard and G. Andre, *J. Phys.: Condens. Matter*, 1995, **7**, 69–87.

53 Y. Tian, M. J. Gray, H. Ji, R. J. Cava and K. S. Burch, *2D Mater.*, 2016, **3**, 025035.

54 Z. Wang, T. Zhang, M. Ding, B. Dong, Y. Li, M. Chen, X. Li, J. Huang, H. Wang, X. Zhao, Y. Li, D. Li, C. Jia, L. Sun, H. Guo, Y. Ye, D. Sun, Y. Chen, T. Yang, J. Zhang, S. Ono, Z. Han and Z. Zhang, *Nat. Nanotechnol.*, 2018, **13**, 554–559.

55 H. J. Deiseroth, K. Aleksandrov, C. Reiner, L. Kienle and R. K. Kremer, *Eur. J. Inorg. Chem.*, 2006, **2006**, 1561–1567.

56 Z. Wang, D. Sapkota, T. Taniguchi, K. Watanabe, D. Mandrus and A. F. Morpurgo, *Nano Lett.*, 2018, **18**, 4303–4308.

57 C. Hu, D. Zhang, F. Yan, Y. Li, Q. Lv, W. Zhu, Z. Wei, K. Chang and K. Wang, *Sci. Bull.*, 2020, **65**, 1072–1077.

58 Y. Deng, Y. Yu, Y. Song, J. Zhang, N. Z. Wang, Z. Sun, Y. Yi, Y. Z. Wu, S. Wu, J. Zhu, J. Wang, X. H. Chen and Y. Zhang, *Nature*, 2018, **563**, 94–99.

59 S. Mangin, D. Ravelosona, J. A. Katine, M. J. Carey, B. D. Terris and E. E. Fullerton, *Nat. Mater.*, 2006, **5**, 210–215.

60 J. Liu, M. Shi, P. Mo and J. Lu, *AIP Adv.*, 2018, **8**, 055316.

61 A. Fert, N. Reyren and V. Cros, *Nat. Rev. Mater.*, 2017, **2**, 1–15.

62 H. H. Kim, B. Yang, T. Patel, F. Sfigakis, C. Li, S. Tian, H. Lei and A. W. Tsen, *Nano Lett.*, 2018, **18**, 4885–4890.

63 T. Song, M. W. Y. Tu, C. Carnahan, X. Cai, T. Taniguchi, K. Watanabe, M. A. McGuire, D. H. Cobden, D. Xiao, W. Yao and X. Xu, *Nano Lett.*, 2019, **19**(2), 915–920.

64 H. H. Kim, B. Yang, S. Tian, C. Li, G. X. Miao, H. Lei and A. W. Tsen, *Nano Lett.*, 2019, **19**, 5739–5745.

65 S. Jiang, L. Li, Z. Wang, J. Shan and K. F. Mak, *Nat. Electron.*, 2019, **2**, 159–163.

66 A. V. Chumak, V. I. Vasyuchka, A. A. Serga and B. Hillebrands, *Nat. Phys.*, 2015, **11**, 453–461.

67 R. Lebrun, A. Ross, S. A. Bender, A. Qaiumzadeh, L. Baldrati, J. Cramer, A. Brataas, R. A. Duine and M. Kläui, *Nature*, 2018, **561**, 222–225.

68 W. Xing, L. Qiu, X. Wang, Y. Yao, Y. Ma, R. Cai, S. Jia, X. C. Xie and W. Han, *Phys. Rev. X*, 2019, **9**, 011026.

69 V. Ostwal, T. Shen and J. Appenzeller, *Adv. Mater.*, 2020, **32**, 1906021.

70 T. Dietl and H. Ohno, *Rev. Mod. Phys.*, 2014, **86**, 187–251.

71 M. W. Lin, H. L. Zhuang, J. Yan, T. Z. Ward, A. A. Puretzky, C. M. Rouleau, Z. Gai, L. Liang, V. Meunier, B. G. Sumpter, P. Ganesh, P. R. C. Kent, D. B. Geohegan, D. G. Mandrus and K. Xiao, *J. Mater. Chem. C*, 2016, **4**, 315–322.

72 C. Tan, J. Lee, S. G. Jung, T. Park, S. Albarakati, J. Partridge, M. R. Field, D. G. McCulloch, L. Wang and C. Lee, *Nat. Commun.*, 2018, **9**, 1–7.

73 N. Ito, T. Kikkawa, J. Barker, D. Hirobe, Y. Shiomi and E. Saitoh, *Phys. Rev. B*, 2019, **100**, 060402.

74 B. Huang, G. Clark, D. R. Klein, D. MacNeill, E. Navarro-Moratalla, K. L. Seyler, N. Wilson, M. A. McGuire, D. H. Cobden, D. Xiao, W. Yao, P. Jarillo-Herrero and X. Xu, *Nat. Nanotechnol.*, 2018, **13**, 544–548.

75 L. Webster and J. A. Yan, *Phys. Rev. B*, 2018, **98**, 144411.

76 Y. Kubota, H. Tanaka, T. Ono, Y. Narumi and K. Kindo, *Phys. Rev. B: Condens. Matter Mater. Phys.*, 2015, **91**, 094422.

77 G. Long, T. Zhang, X. Cai, J. Hu, C. W. Cho, S. Xu, J. Shen, Z. Wu, T. Han, J. Lin, J. Wang, Y. Cai, R. Lortz, Z. Mao and N. Wang, *ACS Nano*, 2017, **11**, 11330–11336.

78 J. U. Lee, S. Lee, J. H. Ryoo, S. Kang, T. Y. Kim, P. Kim, C. H. Park, J. G. Park and H. Cheong, *Nano Lett.*, 2016, **16**, 7433–7438.

79 M. R. Habib, S. Wang, W. Wang, H. Xiao, S. M. Obaidulla, A. Gayen, Y. Khan, H. Chen and M. Xu, *Nanoscale*, 2019, **11**, 20123–20132.

80 J. Sugiyama, H. Nozaki, I. Umegaki, T. Uyama, K. Miwa, J. H. Brewer, S. Kobayashi, C. Michioka, H. Ueda and K. Yoshimura, *Phys. Rev. B*, 2016, **94**, 014408.

81 H. Zhang, L. M. Liu and W. M. Lau, *J. Mater. Chem. A*, 2013, **1**, 10821–10828.

82 Z. Zhang, Y. Gong, X. Zou, P. Liu, P. Yang, J. Shi, L. Zhao, Q. Zhang, L. Gu and Y. Zhang, *ACS Nano*, 2019, **13**(1), 885–893.

83 A. Little, C. Lee, C. John, S. Doyle, E. Maniv, N. L. Nair, W. Chen, D. Rees, J. W. F. Venderbos, R. Fernandes, J. G. Analytis and J. Orenstein, *Nat. Mater.*, 2020, **2019**, 1–6.

84 A. N. Andriotis and M. Menon, *Phys. Rev. B: Condens. Matter Mater. Phys.*, 2014, **90**, 125304.

85 J. Zhou, J. Lin, H. Sims, C. Jiang, C. Cong, J. A. Brehm, Z. Zhang, L. Niu, Y. Chen, Y. Zhou, Y. Wang, F. Liu, C. Zhu, T. Yu, K. Suenaga, R. Mishra, S. T. Pantelides, Z. G. Zhu, W. Gao, Z. Liu and W. Zhou, *Adv. Mater.*, 2020, **32**, 1906536.

86 Y.-C. Lin, B. Jariwala, B. M. Bersch, K. Xu, Y. Nie, B. Wang, S. M. Eichfeld, X. Zhang, T. H. Choudhury, Y. Pan, R. Addou, C. M. Smyth, J. Li, K. Zhang, M. A. Haque, S. Fölsch, R. M. Feenstra, R. M. Wallace, K. Cho, S. K. Fullerton-Shirey, J. M. Redwing and J. A. Robinson, *ACS Nano*, 2018, **12**, 965–975.

87 K. Kang, S. Xie, L. Huang, Y. Han, P. Y. Huang, K. F. Mak, C. J. Kim, D. Muller and J. Park, *Nature*, 2015, **520**, 656–660.

88 D. C. Freitas, R. Weht, A. Sulpice, G. Remenyi, P. Strobel, F. Gay, J. Marcus and M. Núñez-Regueiro, *J. Phys.: Condens. Matter*, 2015, **27**, 176002.

89 D. Gao, Q. Xue, X. Mao, W. Wang, Q. Xu and D. Xue, *J. Mater. Chem. C*, 2013, **1**, 5909–5916.

90 M. Bonilla, S. Kolekar, Y. Ma, H. C. Diaz, V. Kalappattil, R. Das, T. Eggers, H. R. Gutierrez, M. H. Phan and M. Batzill, *Nat. Nanotechnol.*, 2018, **13**, 289–293.

91 Z. Fei, B. Huang, P. Malinowski, W. Wang, T. Song, J. Sanchez, W. Yao, D. Xiao, X. Zhu, A. F. May, W. Wu, D. H. Cobden, J. H. Chu and X. Xu, *Nat. Mater.*, 2018, **17**, 778–782.

92 M. A. McGuire, G. Clark, S. Kc, W. M. Chance, G. E. Jellison, V. R. Cooper, X. Xu and B. C. Sales, *Phys. Rev. Mater.*, 2017, **1**, 014001.

93 Z. Zhang, J. Shang, C. Jiang, A. Rasmita, W. Gao and T. Yu, *Nano Lett.*, 2019, **19**, 3138–3142.

94 Y. J. Sun, Q. H. Tan, X. L. Liu, Y. F. Gao and J. Zhang, *J. Phys. Chem. Lett.*, 2019, **10**, 3087–3093.

95 K. Kim, S. Y. Lim, J. U. Lee, S. Lee, T. Y. Kim, K. Park, G. S. Jeon, C. H. Park, J. G. Park and H. Cheong, *Nat. Commun.*, 2019, **10**, 345.

96 A. Wiedenmann, J. Rossat-Mignod, A. Louisy, R. Brec and J. Rouxel, *Solid State Commun.*, 1981, **40**, 1067–1072.

97 V. Carteaux, F. Moussa and M. Spiesser, *EPL*, 1995, **29**, 251–256.

98 D. A. Estyunin, I. I. Klimovskikh, A. M. Shikin, E. F. Schwier, M. M. Otrokov, A. Kimura, S. Kumar, S. O. Filnov, Z. S. Aliev, M. B. Babanly and E. V. Chulkov, *APL Mater.*, 2020, **8**, 021105.

99 S. Sinn, C. H. Kim, B. H. Kim, K. D. Lee, C. J. Won, J. S. Oh, M. Han, Y. J. Chang, N. Hur, H. Sato, B. G. Park, C. Kim, H. Do Kim and T. W. Noh, *Sci. Rep.*, 2016, **6**, 1–7.

100 H. B. Cao, A. Banerjee, J. Q. Yan, C. A. Bridges, M. D. Lumsden, D. G. Mandrus, D. A. Tennant, B. C. Chakoumakos and S. E. Nagler, *Phys. Rev. B*, 2016, **93**, 134423.

101 C. Gong and X. Zhang, *Science*, 2019, **363**, eaav4450.

102 D. Ghazaryan, M. T. Greenaway, Z. Wang, V. H. Guarochico-Moreira, I. J. Vera-Marun, J. Yin, Y. Liao, S. V. Morozov, O. Kristanovski, A. I. Lichtenstein, M. I. Katsnelson, F. Withers, A. Mishchenko, L. Eaves, A. K. Geim, K. S. Novoselov and A. Misra, *Nat. Electron.*, 2018, **1**, 344–349.

103 X. Cai, T. Song, N. P. Wilson, G. Clark, M. He, X. Zhang, T. Taniguchi, K. Watanabe, W. Yao, D. Xiao, M. A. McGuire, D. H. Cobden and X. Xu, *Nano Lett.*, 2019, **19**, 3993–3998.

104 T. Li, S. Jiang, N. Sivadas, Z. Wang, Y. Xu, D. Weber, J. E. Goldberger, K. Watanabe, T. Taniguchi, C. J. Fennie, K. Fai Mak and J. Shan, *Nat. Mater.*, 2019, **18**, 1303–1308.

105 S. Jiang, L. Li, Z. Wang, K. F. Mak and J. Shan, *Nat. Nanotechnol.*, 2018, **13**, 549–553.

106 M. Grönke, B. Buschbeck, P. Schmidt, M. Valldor, S. Oswald, Q. Hao, A. Lubk, D. Wolf, U. Steiner, B. Büchner and S. Hampel, *Adv. Mater. Interfaces*, 2019, **6**, 1901410.

107 M. A. McGuire, H. Dixit, V. R. Cooper and B. C. Sales, *Chem. Mater.*, 2015, **27**, 612–620.

108 M. Abramchuk, S. Jaszewski, K. R. Metz, G. B. Osterhoudt, Y. Wang, K. S. Burch and F. Tafti, *Adv. Mater.*, 2018, **30**, 1801325.

109 T. Zhang, Y. Wang, H. Li, F. Zhong, J. Shi, M. Wu, Z. Sun, W. Shen, B. Wei, W. Hu, X. Liu, L. Huang, C. Hu, Z. Wang, C. Jiang, S. Yang, Q. M. Zhang and Z. Qu, *ACS Nano*, 2019, **13**, 11353–11362.

110 M. C. De Siena, S. E. Creutz, A. Regan, P. Malinowski, Q. Jiang, K. T. Kluherz, G. Zhu, Z. Lin, J. J. De Yoreo, X. Xu, J. H. Chu and D. R. Gamelin, *Nano Lett.*, 2020, **20**, 2100–2106.

111 C. Song, X. Liu, X. Wu, J. Wang, J. Pan, T. Zhao, C. Li and J. Wang, *J. Appl. Phys.*, 2019, **126**, 105111.

112 J. Wu, F. Liu, C. Liu, Y. Wang, C. Li, Y. Lu, S. Matsuishi and H. Hosono, *Adv. Mater.*, 2020, **32**, 2001815.

113 M. Mogi, A. Tsukazaki, Y. Kaneko, R. Yoshimi, K. S. Takahashi, M. Kawasaki and Y. Tokura, *APL Mater.*, 2018, **6**, 091104.

114 X. Zhou, B. Brzostowski, A. Durajski, M. Liu, J. Xiang, T. Jiang, Z. Wang, S. Chen, P. Li, Z. Zhong, A. Drzewiński, M. Jarosik, R. Szczęśniak, T. Lai, D. Guo and D. Zhong, *J. Phys. Chem. C*, 2020, **124**, 9416–9423.

115 R. D. McAuliffe, G. Yang, J. Nanda and G. M. Veith, *Thin Solid Films*, 2019, **689**, 137520.

116 Q. Sun and N. Kioussis, *Phys. Rev. B*, 2018, **97**, 094408.

117 H. Liu, X. Wang, J. Wu, Y. Chen, J. Wan, R. Wen, J. Yang, Y. Liu, Z. Song and L. Xie, *ACS Nano*, 2020, **14**, 10544–10551.

118 D. G. Wiesler, H. Zabel and S. M. Shapiro, *Phys. B*, 1989, **156–157**, 292–294.

119 I. Eremin, P. Thalmeier, P. Fulde, R. K. Kremer, K. Ahn and A. Simon, *Phys. Rev. B: Condens. Matter Mater. Phys.*, 2001, **64**, 644251–644256.

120 H. A. Krug von Nidda, A. Loidl, K. Ahn, R. K. Kremer and A. Simon, *Phys. Rev. B: Condens. Matter Mater. Phys.*, 2004, **69**, 104407.

121 Z. Ropka, R. Michalski and R. J. Radwanski, *Phys. Rev. B: Condens. Matter Mater. Phys.*, 2001, **63**, 172404.

122 S. J. Youn, B. R. Sahu and K. S. Kim, *Phys. Rev. B: Condens. Matter Mater. Phys.*, 2002, **65**, 524151–524154.

123 B. L. Chittari, D. Lee, N. Banerjee, A. H. MacDonald, E. Hwang and J. Jung, *Phys. Rev. B*, 2020, **101**, 085415.

124 B. Chen, J. H. Yang, H. D. Wang, M. Imai, H. Ohta, C. Michioka, K. Yoshimura and M. H. Fang, *J. Phys. Soc. Jpn.*, 2013, **82**, 124711.

125 M. S. Baranava, D. C. Hvazdouski, V. A. Skachkova, V. R. Stempitsky and A. L. Danilyuk, in *Materials Today: Proceedings*, Elsevier Ltd, 2018, vol. 20, pp. 342–347.

126 Y. Liu and C. Petrovic, *Phys. Rev. Mater.*, 2019, **3**, 014001.

127 H. Ji, R. A. Stokes, L. D. Alegria, E. C. Blomberg, M. A. Tanatar, A. Reijnders, L. M. Schoop, T. Liang, R. Prozorov, K. S. Burch, N. P. Ong, J. R. Petta and R. J. Cava, *J. Appl. Phys.*, 2013, **114**, 114907.

128 L. D. Casto, A. J. Clune, M. O. Yokosuk, J. L. Musfeldt, T. J. Williams, H. L. Zhuang, M. W. Lin, K. Xiao, R. G. Hennig, B. C. Sales, J. Q. Yan and D. Mandrus, *APL Mater.*, 2015, **3**, 041515.

129 Y. Deng, Y. Yu, M. Z. Shi, Z. Guo, Z. Xu, J. Wang, X. H. Chen and Y. Zhang, *Science*, 2020, **367**, 895–900.

130 Z. S. Aliev, I. R. Amiraslanov, D. I. Nasonova, A. V. Shevelkov, N. A. Abdullayev, Z. A. Jahangirli, E. N. Orujlu, M. M. Otrokov, N. T. Mamedov, M. B. Babanly and E. V. Chulkov, *J. Alloys Compd.*, 2019, **789**, 443–450.

131 A. Zeugner, F. Nietschke, A. U. B. Wolter, S. Gaß, R. C. Vidal, T. R. F. Peixoto, D. Pohl, C. Damm, A. Lubk, R. Hentrich, S. K. Moser, C. Fornari, C. H. Min, S. Schatz, K. Kißner, M. Ünzelmann, M. Kaiser, F. Scaravaggi, B. Rellinghaus, K. Nielsch, C. Hess, B. Büchner, F. Reinert, H. Bentmann, O. Oeckler, T. Doert, M. Ruck and A. Isaeva, *Chem. Mater.*, 2019, **31**, 2795–2806.

132 S. Lei, J. Lin, Y. Jia, M. Gray, A. Topp, G. Farahi, S. Klemenz, T. Gao, F. Rodolakis, J. L. McChesney, C. R. Ast, A. Yazdani, K. S. Burch, S. Wu, N. P. Ong and L. M. Schoop, *Sci. Adv.*, 2020, **6**, eaay6407.

133 L. Kang, C. Ye, X. Zhao, X. Zhou, J. Hu, Q. Li, D. Liu, C. M. Das, J. Yang, D. Hu, J. Chen, X. Cao, Y. Zhang, M. Xu, J. Di, D. Tian, P. Song, G. Kutty, Q. Zeng, Q. Fu, Y. Deng, J. Zhou, A. Ariando, F. Miao, G. Hong, Y. Huang, S. J. Pennycook, K. T. Yong, W. Ji, X. Renshaw Wang and Z. Liu, *Nat. Commun.*, 2020, **11**, 1–9.

134 R. A. Patil, H. W. Tu, M. H. Jen, J. J. Lin, C. C. Wu, C. C. Yang, D. Van Pham, C. H. Tsai, C. C. Lai, Y. Liou, W. Bin Jian and Y. R. Ma, *Mater. Today Phys.*, 2020, **12**, 100174.

135 X. Wang, J. Tang, X. Xia, C. He, J. Zhang, Y. Liu, C. Wan, C. Fang, C. Guo, W. Yang, Y. Guang, X. Zhang, H. Xu, J. Wei, M. Liao, X. Lu, J. Feng, X. Li, Y. Peng, H. Wei, R. Yang, D. Shi, X. Zhang, Z. Han, Z. Zhang, G. Zhang, G. Yu and X. Han, *Sci. Adv.*, 2019, **5**, eaaw8904.

136 T. A. Shifa, F. Wang, Z. Cheng, P. He, Y. Liu, C. Jiang, Z. Wang and J. He, *Adv. Funct. Mater.*, 2018, **28**, 1800548.

137 S. Fan, S. J. Yun, W. J. Yu and Y. H. Lee, *Adv. Sci.*, 2020, **7**, 1902751.

138 M. A. Susner, M. Chyasnavichyus, M. A. McGuire, P. Ganesh and P. Maksymovych, *Adv. Mater.*, 2017, **29**, 1602852.

139 F. Wang, T. A. Shifa, P. Yu, P. He, Y. Liu, F. Wang, Z. Wang, X. Zhan, X. Lou, F. Xia and J. He, *Adv. Funct. Mater.*, 2018, **28**, 1802151.

140 T. Masubuchi, H. Hoya, T. Watanabe, Y. Takahashi, S. Ban, N. Ohkubo, K. Takase and Y. Takano, *J. Alloys Compd.*, 2008, **460**, 668–674.

141 V. Maisonneuve, M. Evain, C. Payen, V. B. Cajipe and P. Molinié, *J. Alloys Compd.*, 1995, **218**, 157–164.

142 F. Wang, T. A. Shifa, P. He, Z. Cheng, J. Chu, Y. Liu, Z. Wang, F. Wang, Y. Wen, L. Liang and J. He, *Nano Energy*, 2017, **40**, 673–680.

143 J. Chu, F. Wang, L. Yin, L. Lei, C. Yan, F. Wang, Y. Wen, Z. Wang, C. Jiang, L. Feng, J. Xiong, Y. Li and J. He, *Adv. Funct. Mater.*, 2017, **27**, 1701342.

144 Z. Cheng, M. G. Sendeku and Q. Liu, *Nanotechnology*, 2020, **31**, 135405.

145 H. Huang, M. Shang, Y. Zou, W. Song and Y. Zhang, *Nanoscale*, 2019, **11**, 21188–21195.

146 K. Du, X. Wang, Y. Liu, P. Hu, M. I. B. Utama, C. K. Gan, Q. Xiong and C. Kloc, *ACS Nano*, 2016, **10**, 1738–1743.

147 S. J. Yun, D. L. Duong, D. M. Ha, K. Singh, T. L. Phan, W. Choi, Y. Kim and Y. H. Lee, *Adv. Sci.*, 2020, 1903076.

148 D. C. Freitas, M. Núñez, P. Strobel, A. Sulpice, R. Weht, A. A. Aligia and M. Núñez-Regueiro, *Phys. Rev. B: Condens. Matter Mater. Phys.*, 2013, **87**, 014420.

149 A. Purbawati, J. Coraux, J. Vogel, A. Hadj-Azzem, N. Wu, N. Bendiab, D. Jegouso, J. Renard, L. Marty, V. Bouchiat, A. Sulpice, L. Aballe, M. Foerster, F. Genuzio, A. Locatelli, T. O. Menteş, Z. Han, X. Sun, M. Núñez-Regueiro and N. Rougemaille, *ACS Appl. Mater. Interfaces*, 2020, **12**(27), 30702–30710.

150 C. Wang, X. Zhou, Y. Pan, J. Qiao, X. Kong, C. C. Kaun and W. Ji, *Phys. Rev. B*, 2018, **97**, 245409.

151 H. Liu, Y. Xue, J. A. Shi, R. A. Guzman, P. Zhang, Z. Zhou, Y. He, C. Bian, L. Wu, R. Ma, J. Chen, J. Yan, H. Yang, C. M. Shen, W. Zhou, L. Bao and H. J. Gao, *Nano Lett.*, 2019, **19**, 8572–8580.

152 H. Zhang, L. Sun, Y. Dai, C. Tong and X. Han, *J. Wuhan Univ. Technol., Mater. Sci. Ed.*, 2017, **32**, 574–578.

153 A. V. Ushakov, D. A. Kukusta, A. N. Yaresko and D. I. Khomskii, *Phys. Rev. B: Condens. Matter Mater. Phys.*, 2013, **87**, 014418.

154 A. Shivayogimath, J. D. Thomsen, D. M. A. Mackenzie, M. Geisler, R. M. Stan, A. J. Holt, M. Bianchi, A. Crovetto,

P. R. Whelan, A. Carvalho, A. H. C. Neto, P. Hofmann, N. Stenger, P. Bøggild and T. J. Booth, *Nat. Commun.*, 2019, **10**, 1–7.

155 X. Li, W. Cai, J. An, S. Kim, J. Nah, D. Yang, R. Piner, A. Velamakanni, I. Jung, E. Tutuc, S. K. Banerjee, L. Colombo and R. S. Ruoff, *Science*, 2009, **324**, 1312–1314.

156 Y. Gao, Z. Liu, D. M. Sun, L. Huang, L. P. Ma, L. C. Yin, T. Ma, Z. Zhang, X. L. Ma, L. M. Peng, H. M. Cheng and W. Ren, *Nat. Commun.*, 2015, **6**, 1–10.

157 J. Zhou, J. Lin, X. Huang, Y. Zhou, Y. Chen, J. Xia, H. Wang, Y. Xie, H. Yu, J. Lei, D. Wu, F. Liu, Q. Fu, Q. Zeng, C. H. Hsu, C. Yang, L. Lu, T. Yu, Z. Shen, H. Lin, B. I. Yakobson, Q. Liu, K. Suenaga, G. Liu and Z. Liu, *Nature*, 2018, **556**, 355–359.

158 S. S. Li, S. F. Wang, D. M. Tang, W. J. Zhao, H. L. Xu, L. Q. Chu, Y. Bando, D. Golberg and G. Eda, *Appl. Mater. Today*, 2015, **1**(1), 60–66.

159 S. H. Yu, Z. Tang, Y. Shao, H. Dai, H. Y. Wang, J. Yan, H. Pan and D. H. C. Chua, *ACS Appl. Energy Mater.*, 2019, **2**, 5799–5808.

160 J. Li, B. Zhao, P. Chen, R. Wu, B. Li, Q. Xia, G. Guo, J. Luo, K. Zang, Z. Zhang, H. Ma, G. Sun, X. Duan and X. Duan, *Adv. Mater.*, 2018, **30**, 1801043.

161 D. Ma, W. Ju, T. Li, X. Zhang, C. He, B. Ma, Y. Tang, Z. Lu and Z. Yang, *Appl. Surf. Sci.*, 2016, **364**, 181–189.

162 A. Ramasubramaniam and D. Naveh, *Phys. Rev. B: Condens. Matter Mater. Phys.*, 2013, **87**, 195201.

163 V. Caciuc, N. Atodiresei and S. Blügel, *Phys. Rev. Mater.*, 2018, **2**, 084001.

164 H. Shu, P. Luo, P. Liang, D. Cao and X. Chen, *ACS Appl. Mater. Interfaces*, 2015, **7**, 7534–7541.

165 S. Ahmed, X. Ding, P. P. Murmu, N. Bao, R. Liu, J. Kennedy, L. Wang, J. Ding, T. Wu, A. Vinu and J. Yi, *Small*, 2020, **16**, 1903173.

166 Y. Yamasaki, R. Moriya, M. Arai, S. Masubuchi, S. Pyon, T. Tamegai, K. Ueno and T. Machida, *2D Mater.*, 2017, **4**, 041007.

167 N. Sirica, P. Vilmercati, F. Bondino, I. Pis, S. Nappini, S. K. Mo, A. V. Fedorov, P. K. Das, I. Vobornik, J. Fujii, L. Li, D. Sapkota, D. S. Parker, D. G. Mandrus and N. Mannella, *Commun. Phys.*, 2020, **3**, 1–8.

168 N. J. Ghimire, M. A. McGuire, D. S. Parker, B. Sipos, S. Tang, J. Q. Yan, B. C. Sales and D. Mandrus, *Phys. Rev. B: Condens. Matter Mater. Phys.*, 2013, **87**, 104403.

169 K. Lu, D. Sapkota, L. DeBeer-Schmitt, Y. Wu, H. B. Cao, N. Mannella, D. Mandrus, A. A. Aczel and G. J. MacDougall, *Phys. Rev. Mater.*, 2020, **4**, 054416.

170 K. Zhang, S. Feng, J. Wang, A. Azcatl, N. Lu, R. Addou, N. Wang, C. Zhou, J. Lerach, V. Bojan, M. J. Kim, L. Q. Chen, R. M. Wallace, M. Terrones, J. Zhu and J. A. Robinson, *Nano Lett.*, 2015, **15**, 6586–6591.

171 S. K. Pandey, H. Alsalman, J. G. Azadani, N. Izquierdo, T. Low and S. A. Campbell, *Nanoscale*, 2018, **10**, 21374–21385.

172 K. Zhang and J. A. Robinson, *MRS Adv.*, 2019, **4**, 2743–2757.

173 S. J. Yun, D. L. Duong, D. M. Ha, K. Singh, T. L. Phan, W. Choi, Y. Kim and Y. H. Lee, *Adv. Sci.*, 2020, **7**, 1903076.

174 Y. T. H. Pham, M. Liu, V. O. Jimenez, Z. Yu, V. Kalappattil, F. Zhang, K. Wang, T. Williams, M. Terrones and M. Phan, *Adv. Mater.*, 2020, 2003607.

175 X. Li, C. W. Magnuson, A. Venugopal, R. M. Tromp, J. B. Hannon, E. M. Vogel, L. Colombo and R. S. Ruoff, *J. Am. Chem. Soc.*, 2011, **133**, 2816–2819.

176 Y. Shi, C. Hamsen, X. Jia, K. K. Kim, A. Reina, M. Hofmann, A. L. Hsu, K. Zhang, H. Li, Z. Y. Juang, M. S. Dresselhaus, L. J. Li and J. Kong, *Nano Lett.*, 2010, **10**, 4134–4139.

177 K. K. Liu, W. Zhang, Y. H. Lee, Y. C. Lin, M. T. Chang, C. Y. Su, C. S. Chang, H. Li, Y. Shi, H. Zhang, C. S. Lai and L. J. Li, *Nano Lett.*, 2012, **12**, 1538–1544.

178 P. R. Kidambi, R. Blume, J. Kling, J. B. Wagner, C. Baehtz, R. S. Weatherup, R. Schloegl, B. C. Bayer and S. Hofmann, *Chem. Mater.*, 2014, **26**, 6380–6392.

179 Z. Cai, B. Liu, X. Zou and H.-M. Cheng, *Chem. Rev.*, 2018, **118**, 6091–6133.

180 S. M. Shinde, T. Das, A. T. Hoang, B. K. Sharma, X. Chen and J.-H. Ahn, *Adv. Funct. Mater.*, 2018, **28**, 1706231.

181 X. Zhang, S. Lee, A. Bansal, F. Zhang, M. Terrones, T. N. Jackson and J. M. Redwing, *J. Cryst. Growth*, 2020, **533**, 125471.

182 A. Kozhakhmetov, T. H. Choudhury, Z. Y. Al Balushi, M. Chubarov and J. M. Redwing, *J. Cryst. Growth*, 2018, **486**, 137–141.

183 A. T. Barton, R. Yue, L. A. Walsh, G. Zhou, C. Cormier, C. M. Smyth, R. Addou, L. Colombo, R. M. Wallace and C. L. Hinkle, *2D Mater.*, 2019, **6**, 045027.

184 S. Vishwanath, X. Liu, S. Rouvimov, P. C. Mende, A. Azcatl, S. McDonnell, R. M. Wallace, R. M. Feenstra, J. K. Furdyna, D. Jena and H. G. Xing, *2D Mater.*, 2015, **2**, 024007.

185 R. Yue, Y. Nie, L. A. Walsh, R. Addou, C. Liang, N. Lu, A. T. Barton, H. Zhu, Z. Che, D. Barrera, L. Cheng, P.-R. Cha, Y. J. Chabal, J. W. P. Hsu, J. Kim, M. J. Kim, L. Colombo, R. M. Wallace, K. Cho and C. L. Hinkle, *2D Mater.*, 2017, **4**, 045019.

186 W. Hao, C. Marichy and C. Journet, *2D Mater.*, 2019, **6**, 12001.

187 L. K. Tan, B. Liu, J. H. Teng, S. Guo, H. Y. Low and K. P. Loh, *Nanoscale*, 2014, **6**, 10584–10588.

188 L. Liu, Y. Huang, J. Sha and Y. Chen, *Nanotechnology*, 2017, **28**, 195605.

189 M. Ritala, J. Niinisto, S. Krumdieck, P. Chalker, H. Aspinall, M. E. Pemble, W. L. Gladfelter, B. Leese, R. A. Fischer, H. Parala, R. Kanjolia, R. D. Dupuis, S. E. Alexandrov, S. J. C. Irvine, R. Palgrave, I. P. Parkin, A. C. Jones and M. L. Hitchman, *Chemical Vapour Deposition*, The Royal Society of Chemistry, 2009.

190 M. Razeghi, *The MOCVD Challenge*, CRC Press, 2nd edn, 2011.

191 K. Momeni, Y. Ji, Y. Wang, S. Paul, S. Neshani, D. E. Yilmaz, Y. K. Shin, D. Zhang, J. W. Jiang, H. S. Park, S. Sinnott, A. van Duin, V. Crespi and L. Q. Chen, *npj Comput. Mater.*, 2020, **6**, 1–18.

192 S. M. Eichfeld, V. O. Colon, Y. Nie, K. Cho and J. A. Robinson, *2D Mater.*, 2016, **3**, 025015.

193 Y. Nie, C. Liang, P. R. Cha, L. Colombo, R. M. Wallace and K. Cho, *Sci. Rep.*, 2017, **7**, 1–13.

194 K. Momeni, Y. Ji, K. Zhang, J. A. Robinson and L.-Q. Chen, *npj 2D Mater. Appl.*, 2018, **2**, 27.

195 S. K. Ghandhi and R. J. Field, *J. Cryst. Growth*, 1984, **69**, 619–622.

196 A. G. Salinger, J. N. Shadid, S. A. Scott, G. L. Hennigan, K. D. Devine and H. K. Moffat, *J. Cryst. Growth*, 1999, **203**, 516–533.

197 T. S. Cheng and M. C. Hsiao, *J. Cryst. Growth*, 2008, **310**, 3097–3106.

198 L. Tang, T. Li, Y. Luo, S. Feng, Z. Cai, H. Zhang, B. Liu and H.-M. Cheng, *ACS Nano*, 2020, **14**(4), 4646–4653.

199 S. M. Eichfeld, L. Hossain, Y.-C. Lin, A. F. Piasecki, B. Kupp, A. G. Birdwell, R. A. Burke, N. Lu, X. Peng, J. Li, A. Azcatl, S. McDonnell, R. M. Wallace, M. J. Kim, T. S. Mayer, J. M. Redwing and J. A. Robinson, *ACS Nano*, 2015, **9**, 2080–2087.

200 X. Zhang, T. H. Choudhury, M. Chubarov, Y. Xiang, B. Jariwala, F. Zhang, N. Alem, G. C. Wang, J. A. Robinson and J. M. Redwing, *Nano Lett.*, 2018, **18**, 1049–1056.

201 Y. C. Lin, B. Jariwala, B. M. Bersch, K. Xu, Y. Nie, B. Wang, S. M. Eichfeld, X. Zhang, T. H. Choudhury, Y. Pan, R. Addou, C. M. Smyth, J. Li, K. Zhang, M. A. Haque, S. Folsch, R. M. Feenstra, R. M. Wallace, K. Cho, S. K. Fullerton-Shirey, J. M. Redwing and J. A. Robinson, *ACS Nano*, 2018, **12**, 965–975.

202 X. Zhang, F. Zhang, Y. Wang, D. S. Schulman, T. Zhang, A. Bansal, N. Alem, S. Das, V. H. Crespi, M. Terrones and J. M. Redwing, *ACS Nano*, 2019, **13**(3), 3341–3352.

203 T. H. Choudhury, H. Simchi, R. Boichot, M. Chubarov, S. E. Mohney and J. M. Redwing, *Cryst. Growth Des.*, 2018, **18**, 4357–4364.

204 A. Govind Rajan, J. H. Warner, D. Blankschtein and M. S. Strano, *ACS Nano*, 2016, **10**, 4330–4344.

205 R. Shi, P. He, X. Cai, Z. Zhang, W. Wang, J. Wang, X. Feng, Z. Wu, A. Amini, N. Wang and C. Cheng, *ACS Nano*, 2020, **14**(6), 7593–7601.

206 X. Zhang, Z. Y. Al Balushi, F. Zhang, T. H. Choudhury, S. M. Eichfeld, N. Alem, T. N. Jackson, J. A. Robinson and J. M. Redwing, *J. Electron. Mater.*, 2016, **45**, 6273–6279.

207 R. Chellappa and D. Chandra, *J. Chem. Thermodyn.*, 2005, **37**, 377–387.

208 W. J. Wei and M. Lo, *Appl. Organomet. Chem.*, 1998, **12**, 201–220.

209 G. Carta, M. Natali, G. Rossetto, P. Zanella, G. Salmaso, S. Restello, V. Rigato, S. Kaciulis and A. Mezzi, *Chem. Vap. Deposition*, 2005, **11**, 375–380.

210 S. Wang, K. A. Owusu, L. Mai, Y. Ke, Y. Zhou, P. Hu, S. Magdassi and Y. Long, *Appl. Energy*, 2018, **211**, 200–217.

211 D. Barreca, *J. Electrochem. Soc.*, 1999, **146**, 551.

212 D. Vernardou, M. E. Pemble and D. W. Sheel, *Surf. Coat. Technol.*, 2004, **188–189**, 250–254.

213 G. N. Pain, G. I. Christiansz, R. S. Dickson, G. B. Deacon, B. O. West, K. McGgregor and R. S. Rowe, *Polyhedron*, 1990, **9**, 921–929.

214 G. I. Christiansz, T. J. Elms, G. N. Pain and R. R. Pierson, *J. Cryst. Growth*, 1988, **93**, 589–593.

215 E. Chikoidze, Y. Dumont, F. Jomard and O. Gorochov, *Thin Solid Films*, 2007, **515**, 8519–8523.

216 P. A. Lane, P. J. Wright, P. E. Oliver, C. L. Reeves, A. D. Pitt, J. M. Keen, M. C. L. Ward, M. E. G. Tilsley, N. A. Smith, B. Cockayne and I. R. Harris, *Chem. Vap. Deposition*, 1997, **3**, 97–101.

217 B. Thomas, T. Cibik, C. Höpfner, K. Diesner, G. Ehlers, S. Fiechter and K. Ellmer, *J. Mater. Sci.: Mater. Electron.*, 1998, **9**, 61–64.

218 C. Pflitsch, D. Viefhaus, U. Bergmann, V. Kravets, H. Nienhaus and B. Atakan, in *Proceedings - Electrochemical Society*, IOP Publishing, 2005, vol. PV 2005-09, pp. 849–856.

219 C. C. Chai, J. Peng and B. P. Yan, *Sens. Actuators, B*, 1996, **34**, 412–416.

220 T. Maruyama and Y. Shinyashiki, *Thin Solid Films*, 1998, **333**, 203–206.

221 P. A. Lane, P. J. Wright, P. E. Oliver, C. L. Reeves, A. D. Pitt, J. M. Keen, M. C. L. Ward, M. E. G. Tilsley, N. A. Smith, B. Cockayne and I. R. Harris, *Chem. Vap. Deposition*, 1997, **3**, 97–101.

222 Z. Shi, *Sci. Total Environ.*, 1994, **148**, 293–298.

223 L. Brissonneau and C. Vahlas, *Chem. Vap. Deposition*, 1999, **5**, 135–142.

224 M. Becht, F. Atamny, A. Baiker and K. H. Dahmen, *Surf. Sci.*, 1997, **371**, 399–408.

225 M. Becht, J. Gallus, M. Hunziker, F. Atamny and K.-H. Dahmen, *Le J. Phys. IV*, 1995, **05**, C5-465–C5-472.

226 A. Giani, A. Boulouz, F. Pascal-Delannoy, A. Foucaran and A. Boyer, *Thin Solid Films*, 1998, **315**, 99–103.

227 A. Giani, A. Boulouz, F. Pascal-Delannoy, A. Foucaran, E. Charles and A. Boyer, *Mater. Sci. Eng., B*, 1999, **64**, 19–24.

228 S. W. Cho, K. C. Kim, S. K. Kim, B. ki Cheong, J. S. Kim and S. Lee, *J. Alloys Compd.*, 2017, **723**, 942–947.

229 I. S. Chen, J. F. Roeder, T. E. Glassman and T. H. Baum, *Chem. Mater.*, 1999, **11**, 209–212.

230 Y. Senzaki, A. K. Hochberg and J. A. T. Norman, *Adv. Mater. Opt. Electron.*, 2000, **10**, 93–103.

231 D. Bekermann, D. Barreca, A. Gasparotto, H. W. Becker, R. A. Fischer and A. Devi, *Surf. Coat. Technol.*, 2009, **204**, 404–409.

232 Y. Chen, R. Singh and J. Narayan, *J. Electron. Mater.*, 1997, **26**, 350–354.

233 M. Lemberger, S. Thiemann, A. Baunemann, H. Parala, R. A. Fischer, J. Hinz, A. J. Bauer and H. Ryssel, *Surf. Coat. Technol.*, 2007, **201**, 9154–9158.

234 D. R. Sadoway and S. N. Flengas, *Can. J. Chem.*, 1976, **54**, 1692–1699.

235 W. Ge, K. Kawahara, M. Tsuji and H. Ago, *Nanoscale*, 2013, **5**, 5773–5778.

236 S. Zhao, T. Hotta, T. Koretsune, K. Watanabe, T. Taniguchi, K. Sugawara, T. Takahashi, H. Shinohara and R. Kitaura, *2D Mater.*, 2016, **3**, 025027.

237 W. Fu, Y. Chen, J. Lin, X. Wang, Q. Zeng, J. Zhou, L. Zheng, H. Wang, Y. He, H. He, Q. Fu, K. Suenaga, T. Yu and Z. Liu, *Chem. Mater.*, 2016, **28**, 7613–7618.

238 H. Cun, M. Macha, H. K. Kim, K. Liu, Y. Zhao, T. LaGrange, A. Kis and A. Radenovic, *Nano Res.*, 2019, **12**, 2646–2652.

239 M. Marx, A. Grundmann, Y. R. Lin, D. Andrzejewski, T. Kümmell, G. Bacher, M. Heuken, H. Kalisch and A. Vescan, in *Journal of Electronic Materials*, Springer, New York LLC, 2018, vol. 47, pp. 910–916.

240 D. Andrzejewski, M. Marx, A. Grundmann, O. Pfingsten, H. Kalisch, A. Vescan, M. Heuken, T. Kümmell and G. Bacher, *Nanotechnology*, 2018, **29**, 295704.

241 K. Kang, K. H. Lee, Y. Han, H. Gao, S. Xie, D. A. Muller and J. Park, *Nature*, 2017, **550**, 229–233.

242 S. M. Eichfeld, L. Hossain, Y.-C. Lin, A. F. Piasecki, B. Kupp, A. G. Birdwell, R. A. Burke, N. Lu, X. Peng, J. Li, A. Azcatl, S. McDonnell, R. M. Wallace, M. J. Kim, T. S. Mayer, J. M. Redwing and J. A. Robinson, *ACS Nano*, 2015, **9**, 2080–2087.

243 G. L. Hansen, J. L. Schmit and T. N. Casselman, *J. Appl. Phys.*, 1982, **53**, 7099–7101.

244 A. Piotrowski, P. Madejczyk, W. Gawron, K. Kłos, J. Pawluczyk, J. Rutkowski, J. Piotrowski and A. Rogalski, *Infrared Phys. Technol.*, 2007, **49**, 173–182.

245 E. R. Gertner, *Annu. Rev. Mater. Sci.*, 1985, **15**, 303–328.

246 K. Cao, W. Jie, G. Zha, T. Tan, Y. Li and R. Hu, *J. Cryst. Growth*, 2018, **498**, 197–201.

247 K. Cohen, S. Stolyarova, N. Amir, A. Chack, R. Beserman, R. Weil and Y. Nemirovsky, *J. Cryst. Growth*, 1999, **198–199**, 1174–1178.

248 S. M. Gates and S. K. Kulkarni, *Appl. Phys. Lett.*, 1991, **58**, 2963–2965.

249 S. M. Gates and S. K. Kulkarni, *Appl. Phys. Lett.*, 1992, **60**, 53–55.

250 H. M. Shieh, T. S. Wu and W. C. Hsu, *J. Cryst. Growth*, 1992, **121**, 665–670.

251 R. Azoulay, L. Dugrand, D. Ankri and E. V. K. Rao, *J. Cryst. Growth*, 1984, **68**, 453–460.

252 K. H. Lee, A. Jandl, Y. H. Tan, E. A. Fitzgerald and C. S. Tan, *AIP Adv.*, 2013, **3**, 092123.

253 F. Henry, B. Armas, C. Combescure, A. Figueras and S. Garelik, *Surf. Coat. Technol.*, 1996, **80**, 134–138.

254 S. Veintemillas-Verdaguer, A. Figueras and R. Rodriguez-Clemente, *J. Cryst. Growth*, 1993, **128**, 349–353.

255 M. Bosi and G. Attolini, *Prog. Cryst. Growth Charact. Mater.*, 2010, **56**, 146–174.

256 K. B. McAfee, R. A. Laudise and R. S. Hozack, *J. Lightwave Technol.*, 1983, **LT-1**, 555–561.

257 M. J. Ludowise, *J. Appl. Phys.*, 1985, **58**, R31–R55.

258 K. W. Benz, H. Renz, J. Weidlein and M. H. Pilkuhn, *J. Electron. Mater.*, 1981, **10**, 185–192.

259 H. Kato, W. Futako, S. Yamasaki and H. Okushi, in *Diamond and Related Materials*, Elsevier, 2005, vol. 14, pp. 340–343.

260 T. Saito, M. Kameta, K. Kusakabe, S. Morooka, H. Maeda, Y. Hayashi and T. Asano, *Jpn. J. Appl. Phys., Part 2*, 1998, **37**, L543.

261 R. H. Moss and J. S. Evans, *J. Cryst. Growth*, 1981, **55**, 129–134.

262 V. Barrioz, S. J. C. Irvine, E. W. Jones, R. L. Rowlands and D. A. Lamb, *Thin Solid Films*, 2007, **515**, 5808–5813.

263 S. Yamaga, A. Yoshikawa and H. Kasai, *J. Cryst. Growth*, 1990, **106**, 683–689.

264 Y. K. Ko, B. S. Seo, D. S. Park, H. J. Yang, W. H. Lee, P. J. Reucroft and J. G. Lee, *Electrochem. Solid-State Lett.*, 2003, **6**, C141.

265 Hazardous Substances Data Bank (HSDB): 1025 - PubChem https://pubchem.ncbi.nlm.nih.gov/source/hsdb/ 1025, (accessed 11 October 2020).

266 (Methylcyclopentadienyl)manganese(I) tricarbonyl|CAS No. 12108-13-3|Sigma-Aldrich|Sigma-Aldrich https://www. sigmaaldrich.com/catalog/product/aldrich/317632?lang= en&region=GB, (accessed 3 September 2020).

267 D. R. Stull, *Ind. Eng. Chem.*, 1947, **39**, 517–540.

268 M. T. Vieyra-Eusebio and A. Rojas, *J. Chem. Eng. Data*, 2011, **56**, 5008–5018.

269 J. G. Aston, R. M. Kennedy and G. H. Messerly, *J. Am. Chem. Soc.*, 1941, **63**, 2343–2348.

270 D. V. S. Jain and O. P. Yadav, *Indian J. Chem.*, 1973, **11**, 28–30.

271 P. Morávek, M. Fulem, J. Pangrác, E. Hulicius and K. Růžička, *Fluid Phase Equilib.*, 2013, **360**, 106–110.

272 D. Y. Peng and J. Zhao, *J. Chem. Thermodyn.*, 2001, **33**, 1121–1131.

273 D. W. Osborne, R. N. Doescher and D. M. Yost, *J. Am. Chem. Soc.*, 1942, **64**, 169–172.

274 L. S. Brooks, *J. Am. Chem. Soc.*, 1952, **74**, 227–229.

275 U. Karlson, W. T. Frankenberger and W. F. Spencer, *J. Chem. Eng. Data*, 1994, **39**, 608–610.

276 J. E. Hails and S. J. C. Irvine, *J. Cryst. Growth*, 1991, **107**, 319–324.

277 H. R. Kemme and S. I. Kreps, *J. Chem. Eng. Data*, 1969, **14**, 98–102.

278 H. Li, Y. Li, A. Aljarb, Y. Shi and L.-J. Li, *Chem. Rev.*, 2018, **118**(13), 6134–6150.

279 T. H. Choudhury, X. Zhang, Z. Y. Al Balushi, M. Chubarov and J. M. Redwing, *Annu. Rev. Mater. Res.*, 2020, **50**, 155–177.

280 C. Mattevi, H. Kim and M. Chhowalla, *J. Mater. Chem.*, 2011, **21**, 3324–3334.

281 S. Caneva, R. S. Weatherup, B. C. Bayer, B. Brennan, S. J. Spencer, K. Mingard, A. Cabrero-Vilatela, C. Baehtz, A. J. Pollard and S. Hofmann, *Nano Lett.*, 2015, **15**, 1867–1875.

282 S. Caneva, R. S. Weatherup, B. C. Bayer, R. Blume, A. Cabrero-Vilatela, P. Braeuninger-Weimer, M. B. Martin, R. Wang, C. Baehtz, R. Schloegl, J. C. Meyer and S. Hofmann, *Nano Lett.*, 2016, **16**, 1250–1261.

283 S. J. Yun, S. H. Chae, H. Kim, J. C. Park, J. H. Park, G. H. Han, J. S. Lee, S. M. Kim, H. M. Oh, J. Seok, M. S. Jeong, K. K. Kim and Y. H. Lee, *ACS Nano*, 2015, **9**(5), 5510–5519.

284 Y. Gao, Z. Liu, D.-M. Sun, L. Huang, L.-P. Ma, L.-C. Yin, T. Ma, Z. Zhang, X.-L. Ma, L.-M. Peng, H.-M. Cheng and W. Ren, *Nat. Commun.*, 2015, **6**, 8569.

285 P. C. Sherrell, P. Palczynski, M. S. Sokolikova, F. Reale, F. M. Pesci, M. Och and C. Mattevi, *ACS Appl. Energy Mater.*, 2019, **2**(8), 5877–5882.

286 R. J. Chang, Y. Sheng, T. Chen, N. Mkhize, Y. Lu, H. Bhaskaran and J. H. Warner, *ACS Appl. Nano Mater.*, 2019, **2**, 4222–4231.

287 X. Ling, Y. H. Lee, Y. Lin, W. Fang, L. Yu, M. S. Dresselhaus and J. Kong, *Nano Lett.*, 2014, **14**, 464–472.

288 D. Shcherbakov, P. Stepanov, D. Weber, Y. Wang, J. Hu, Y. Zhu, K. Watanabe, T. Taniguchi, Z. Mao, W. Windl, J. Goldberger, M. Bockrath and C. N. Lau, *Nano Lett.*, 2018, **18**, 4214–4219.

289 D. Kim, S. Park, J. Lee, J. Yoon, S. Joo, T. Kim, K. J. Min, S. Y. Park, C. Kim, K. W. Moon, C. Lee, J. Hong and C. Hwang, *Nanotechnology*, 2019, **30**, 245701.

290 F. Reale, P. Palczynski, I. Amit, G. F. Jones, J. D. Mehew, A. Bacon, N. Ni, P. C. Sherrell, S. Agnoli, M. F. Craciun, S. Russo and C. Mattevi, *Sci. Rep.*, 2017, **7**, 14911.

291 S. Li, S. Wang, D.-M. Tang, W. Zhao, H. Xu, L. Chu, Y. Bando, D. Golberg and G. Eda, *Appl. Mater. Today*, 2015, **1**, 60–66.

292 S. Wang, X. Wang and J. H. Warner, *ACS Nano*, 2015, **9**, 5246–5254.

293 J. T. Mlack, P. Masih Das, G. Danda, Y. C. Chou, C. H. Naylor, Z. Lin, N. P. López, T. Zhang, M. Terrones, A. T. C. Johnson and M. Drndic, *Sci. Rep.*, 2017, **7**, 1–8.

294 T. Severs Millard, A. Genco, E. M. Alexeev, S. Randerson, S. Ahn, A. R. Jang, H. Suk Shin and A. I. Tartakovskii, *npj 2D Mater. Appl.*, 2020, **4**, 1–9.

295 P. Chen, W. Xu, Y. Gao, J. H. Warner and M. R. Castell, *ACS Appl. Nano Mater.*, 2018, **1**, 6976–6988.

296 Y. H. Lee, L. Yu, H. Wang, W. Fang, X. Ling, Y. Shi, C. Te Lin, J. K. Huang, M. T. Chang, C. S. Chang, M. Dresselhaus, T. Palacios, L. J. Li and J. Kong, *Nano Lett.*, 2013, **13**, 1852–1857.

297 N. Balakrishnan, E. D. Steer, E. F. Smith, Z. R. Kudrynskyi, Z. D. Kovalyuk, L. Eaves, A. Patanè and P. H. Beton, *2D Mater.*, 2018, **5**, 035026.

298 C. F. van Bruggen, M. B. Vellinga and C. Haas, *J. Solid State Chem.*, 1970, **2**, 303–308.

299 P. Vaqueiro, A. V. Powell, A. I. Coldea, C. A. Steer, I. M. Marshall, S. J. Blundell, J. Singleton and T. Ohtani, *Phys. Rev. B: Condens. Matter Mater. Phys.*, 2001, **64**, 1324021–1324024.

300 S. Zhou, R. Wang, J. Han, D. Wang, H. Li, L. Gan and T. Zhai, *Adv. Funct. Mater.*, 2019, **29**, 1805880.

301 F. Cui, X. Zhao, J. Xu, B. Tang, Q. Shang, J. Shi, Y. Huan, J. Liao, Q. Chen, Y. Hou, Q. Zhang, S. J. Pennycook and Y. Zhang, *Adv. Mater.*, 2020, **32**, 1905896.

302 X. Wang, Y. Sun and K. Liu, *2D Mater.*, 2019, **6**, 042001.

303 F. Fabbri, F. Dinelli, S. Forti, L. Sementa, S. Pace, G. Piccinini, A. Fortunelli, C. Coletti and P. Pingue, *J. Phys. Chem. C*, 2020, **124**(16), 9035–9044.

304 K. Yao, J. D. Femi-Oyetoro, S. Yao, Y. Jiang, L. El Bouanani, D. C. Jones, P. A. Ecton, U. Philipose, M. El Bouanani, B. Rout, A. Neogi and J. M. Perez, *2D Mater.*, 2020, **7**, 015024.

305 J. Gao, B. Li, J. Tan, P. Chow, T. M. Lu and N. Koratkar, *ACS Nano*, 2016, **10**, 2628–2635.

306 J. C. Park, S. J. Yun, H. Kim, J.-H. Park, S. H. Chae, S.-J. An, J.-G. Kim, S. M. Kim, K. K. Kim and Y. H. Lee, *ACS Nano*, 2015, **9**, 6548–6554.

307 J. Li, S. Cheng, Z. Liu, W. Zhang and H. Chang, *J. Phys. Chem. C*, 2018, **122**, 7005–7012.

308 F. Ye, J. Lee, J. Hu, Z. Mao, J. Wei and P. X.-L. Feng, *Small*, 2016, **12**, 5802–5808.

309 Y. Liu, W. Wang, H. Lu, Q. Xie, L. Chen, H. Yin, G. Cheng and X. Wu, *Appl. Surf. Sci.*, 2020, **511**, 145452.

310 Q. Li, Q. Zhou, L. Shi, Q. Chen and J. Wang, *J. Mater. Chem. A*, 2019, **7**, 4291–4312.

311 G. H. Lee, X. Cui, Y. D. Kim, G. Arefe, X. Zhang, C. H. Lee, F. Ye, K. Watanabe, T. Taniguchi, P. Kim and J. Hone, *ACS Nano*, 2015, **9**, 7019–7026.

312 F. Withers, O. Del Pozo-Zamudio, S. Schwarz, S. Dufferwiel, P. M. Walker, T. Godde, A. P. Rooney, A. Gholinia, C. R. Woods, P. Blake, S. J. Haigh, K. Watanabe, T. Taniguchi, I. L. Aleiner, A. K. Geim, V. I. Fal'Ko, A. I. Tartakovskii and K. S. Novoselov, *Nano Lett.*, 2015, **15**, 8223–8228.

313 S. Shree, A. George, T. Lehnert, C. Neumann, M. Benelajla, C. Robert, X. Marie, K. Watanabe, T. Taniguchi, U. Kaiser, B. Urbaszek and A. Turchanin, *2D Mater.*, 2020, **7**, 015011.

314 H. Jeong, D. Y. Kim, J. Kim, S. Moon, N. Han, S. H. Lee, O. F. N. Okello, K. Song, S. Y. Choi and J. K. Kim, *Sci. Rep.*, 2019, **9**, 1–8.

315 S. Sundaram, X. Li, S. Alam, Y. Halfaya, G. Patriarche and A. Ougazzaden, *J. Cryst. Growth*, 2019, **509**, 40–43.

316 S. M. Kim, A. Hsu, M. H. Park, S. H. Chae, S. J. Yun, J. S. Lee, D. H. Cho, W. Fang, C. Lee, T. Palacios, M. Dresselhaus, K. K. Kim, Y. H. Lee and J. Kong, *Nat. Commun.*, 2015, **6**, 1–11.

317 A. K. Dąbrowska, M. Tokarczyk, G. Kowalski, J. Binder, R. Bozek, J. Borysiuk, R. StÈ©pniewski and A. Wysmołek, *2D Mater.*, 2020, **8**, 015017.